10

Characterizing Structure, Defects, and Chemistry

CHAPTER PREVIEW

In this chapter we discuss techniques that can produce useful information about the structure, chemistry, and bonding in ceramics. There are so many characterization methods available that books are written on each one. Because we can't cover all the details or even all the techniques, we give examples and aim at making you aware of the key ones and their applications.

We can group the techniques into six categories.

- Imaging using visible (or nearly visible) light
- Imaging using electrons (mainly scanning and transmission electron microscopy—SEM and TEM, respectively)
- Imaging using sensing [atomic-force microscopy (AFM) and other scanned probes that "sense" a force or field]
- Scattering and diffraction (using X-rays, neutrons, α-particles, electrons)
- Spectroscopy and spectrometry [using X-rays for energy- and wavelength-dispersive spectrometry (EDS and WDS, respectively) Raman, IR, etc.]
- Thermal analysis [measuring changes (e.g., enthalpy) as a function of temperature]

Most of the techniques we describe can be used to study other classes of materials, but our examples are all related to ceramics.

The suitability of a characterization technique depends on the type of information we hope to obtain. It may also be dictated by the size of our sample, what part of the sample is important, and whether we can destroy the sample. Some of the limitations are:

- Reflection techniques examine only surfaces.
- Techniques using electrons require the sample to be in a vacuum.
- Techniques using transmitted electrons generally require the sample to be thin.
- For nanomaterials we need high resolution.

Two questions that we always ask are:

- How much material is required for the analysis?
- Is it destructive or nondestructive?

For example, TEM is invariably destructive, but you need a very small amount of material for the analysis.

10.1 CHARACTERIZING CERAMICS

In characterizing a ceramic—whether it is a single crystal, polycrystalline, or a glass—there are certain types of information that we are interested in obtaining.

- Chemistry. What is the composition, how does it vary within the sample, etc.?
- Structure. Is the ceramic crystalline or glass or a mixture of the two? What polymorph is present?
- Microstructure. Is the structure the same throughout the sample? Polycrystalline ceramics can't be uniform. Even glass can be structurally inhomogeneous.
- Surface. Whether the sample is crystalline or not, the nature of the surface is often particularly important. If the sample is crystalline, then surface orientation may

C.B. Carter and M.G. Norton, *Ceramic Materials: Science and Engineering*,
DOI 10.1007/978-1-4614-3523-5_10,

TABLE 10.1 Summary of Tools for Ceramics Using Chemical Characteristics

Chemical characteristic	*Characterization tool*
Composition	X-ray diffraction (XRD)
	X-ray fluorescence (XRF)
	Neutron activation analysis (NAA)
	Mass spectrometry (Mass Spec)
Elemental distribution/local chemistry	Scanning electron microscope (SEM) with X-ray energy dispersive spectroscopy (XEDS)
	Electron probe microanalysis (EPMA)
	Transmission electron microscopy (TEM) with XEDS
	TEM with electron energy-loss spectroscopy (EELS)
Surface/interface chemistry	X-ray photoelectron spectroscopy (XPS, ESCA)
	Auger electron spectroscopy (AES)
	Secondary ion mass spectroscopy (SIMS)
	Rutherford backscattering spectrometry (RBS)
	Ultraviolet photoelectron spectroscopy (UPS)
	Infrared (IR) spectroscopy
	Raman spectroscopy
Phase changes (e.g., decomposition and dehydration)	Thermomechanical analysis (TMA)
	Thermogravimetric analysis (TGA)
	Differential thermal analysis (DTA)
	Differential scanning calorimetry (DSC)
	Mass Spec (MS)
	In situ XRD

TABLE 10.2 Summary of Tools for Ceramics Using Physical Characteristics

Physical characteristic	*Characterization tool*
Surface area/porosity (see Chapter 20)	Small angle neutron scattering (SANS)
	Small angle X-ray scattering (SAXS)
	Mercury porosimetry
Density homogeneity	VLM
	SEM
	X-ray radiography/CT scan
	Ultrasonography
	Die penetration
Particle/grain size, distribution, morphology, texture	VLM and quantitative stereology
	SEM and quantitative stereology
	Electron backscattering spectroscopy (EBSD)
	TEM
	XRD
Phase identification/ molecular structure	XRD
	EBSD
	FTIR
	Raman spectroscopy
	EXAFS
	Neutron diffraction
	Mössbauer spectroscopy
	Nuclear magnetic resonance (NMR)
Phase transitions (e.g., structural transformations)	DTA
	DSC
	TMA
	In situ XRD

be critical. Even the surface of a glass is different chemically and structurally from the bulk. In nanomaterials, the surface is the most important feature because most of the atoms are there.

- Defects. In crystals we often want to determine dislocation density. In both crystals and glass we may be interested in the nature, concentration, and distribution of point defects. Techniques for characterizing defects are dealt with mainly in their respective chapters.

What we want to know determines which technique we should use. In the following sections our approach is to illustrate the type of information that can be obtained. Most of these methods are applicable not only to ceramics but to other classes of material. However, there are certain special features associated with ceramics.

- Techniques using electrons can be complicated because many ceramics charge locally, thus deflecting an electron beam.
- We are often interested in what happens while ceramics are being processed. Because of the environment or the high temperatures involved, such in situ studies may not be possible with the desired resolution.
- Ceramics are often multicomponent systems; knowing the average composition may not be too useful. Therefore we may need local compositional analysis on a scale that may be in the nanometer range.
- Many ceramics contain light elements (e.g., B, C. N, O), which can be difficult to quantify.
- If we are interested in interfaces, for example, the interface may facet over short (<100 nm) distances; and it may contain steps that are only nanometers high. In studying such interfaces, it is essential that both grains be observed, so techniques requiring the sample to be broken along the interface would not be ideal (though they may be necessary).

Tables 10.1 and 10.2 lists some of the techniques that you might consider to obtain specific information about your material. In most cases, the use of a particular technique depends in part on its availability, and often a combination of techniques is necessary to get the complete picture.

10.2 IMAGING USING VISIBLE-LIGHT, INFRARED, AND ULTRAVIOLET MICROSCOPY

Light interacts with the specimen in many ways; we then study the resulting image contrast. Contrast is produced by reflection, absorption, refraction, polarization, fluorescence, or diffraction. This contrast can be modified by

physically changing the optical components and illumination mode of the microscope. The final image can also be processed, now mainly using computer techniques.

Visible-light microscopy (VLM) is used routinely for all ceramics. VLM is often referred to as optical microscopy, but essentially all microscopy is optical. The magnification of a VLM can range from 10 × (a magnifying glass) to 50 k × using a liquid between the specimen and the lens. Modern VLMs are equipped with digital cameras (video or still) and feed straight into the computer. Ceramics are often transparent, especially (but not necessarily) if they are glass, so we can then use reflected or transmitted light. The sample can be viewed supported on a table or inverted. The inverted microscope has some advantages; in particular, you can attach contacts to, indent into, or support liquids on the free surface. You also have more flexibility with the lighting.

The lateral resolution using VLM is about 250 nm, and the depth of field has a similar value. Because of the poor depth of field of the VLM, we often examine polished surfaces (as in metallography). Vertical resolution can be <1 nm using interference contrast, and this is bettered only by the scanned probe techniques.

VLM is usually available in every laboratory. Although a conventional VLM may cost only $2,000, the best metallographic microscopes can cost >$100,000. There are numerous imaging methods used in VLM, so we list only a few here.

Dark-field. The image is formed using only scattered light (if there is no specimen present, then the image is dark). It is widely used in mineralogy, where multiphase materials are common.

Polarized light. Polarized VLM distinguishes between isotropic and anisotropic materials and provides information on absorption color and boundaries between minerals of differing refractive indices. The technique provides local information on the structure and composition of materials, as shown in Figure 10.1, which is an image of a neodymium-doped yttrium orthovanadate laser crystal. Individual grains, separated by low-angle grain boundaries, are clearly revealed by polarized VLM.

Nomarski (differential interference contrast). The idea here is that we use interference. Contrast is generated by phase differences between two rays (a sample ray and a reference ray). In the Nomarski microscope, the two rays are created after the light has passed through the sample, where path differences occur because of regions having different refractive indices. The ray is split by a prism (called a Wollaston prism); and after passing through a polarizing filter the rays are recombined using a second prism at the image plane. By using a rotating stage, the image contrast can be varied. Using this technique it is possible to create very attractive images because of the enhanced contrast. Nomarski microscopes are more expensive than conventional VLMs because of the cost of the Wollaston prisms.

NSOM (near-field scanning optical microscopy, also known as SNOM). This is a broad and growing topic. The idea is that the resolution in VLM is limited by λ. If the light source is a fiber with an aperture in the end and we detect the reflected/scattered light with the same fiber, then the spatial resolution is determined by the diameter of the fiber. The limitation is that because the aperture diameter is smaller than λ (Figure 10.2) the emerging wave is evanescent, so the signal strength is small. The use of a laser provides the necessary intensity and defines λ. The usefulness of the technique relies on the ceramics sample having suitable features to scatter the light.

NSOM PARAMETERS

Aperture size	25–100 nm
Tip/sample gap	5–50 nm

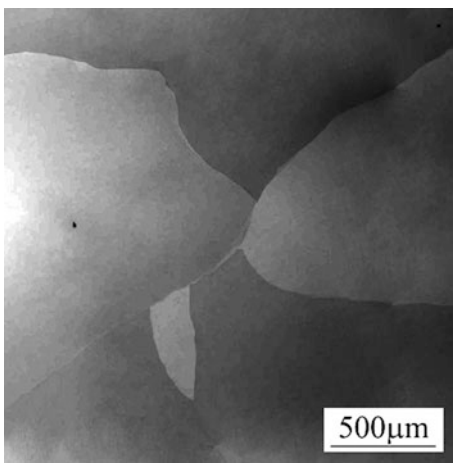

FIGURE 10.1. Slightly misoriented grains in a laser element imaged using polarized visible light microscopy (VLM). The crystal is yttrium orthovanadate with 0.27% Nd.

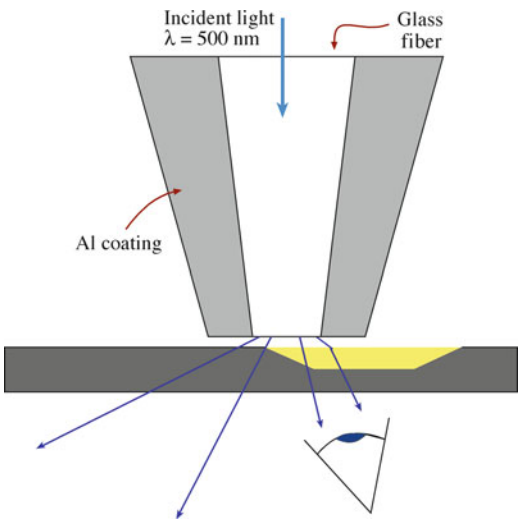

FIGURE 10.2. End of the fiber and the sample, seen by near-field scanning optical microscopy (NSOM).

The technique can be used for other wavelengths and other signals (e.g., Raman). The latter technique is still being developed.

Infrared (IR) and Ultraviolet (UV) microscopy. Because semiconductors are transparent to IR radiation, defects in these materials can be examined with IR microscopy. A detector sensitive to IR is required. With IR and UV light, a converter or detector is also required. An advantage of UV microscopy is that because the wavelength of UV light is smaller than visible light the resolution of these microscopes is higher than VLMs. UV microscopy is widely used in the biological sciences to study subcellular structures. Using intense vacuum UV sources (available at national laboratories), it is possible to obtain results on, for example, electronic states.

10.3 IMAGING USING X-RAYS AND CT SCANS

X-ray topography can be used to obtain images of individual lattice defects in single crystals. This technique has been widely used to study crystal growth, in particular of silicon. It can be used in:

- Reflection (Berg-Barrett method)
- Transmission (Lang method or Borrmann method)

In either method, it is the intensity variation within the diffraction spot that is recorded. It is not usually the defects themselves that are imaged but, rather, the strain fields around them. These strains cause variations in plane spacing from their equilibrium value, thereby modifying the X-ray scattering process. Figure 10.3 shows a Lang topographic image of dislocations in KDP, or potassium dihydrogen phosphate (KH_2PO_4). KDP has a relatively large electro-optic effect and can be grown as large strain-free crystals. X-ray topography has several advantages for characterizing defects in single crystals. It is nondestructive, does not require ultra-thin samples (as we do in TEM), and can be used to observe very low dislocation densities (limit in TEM $>10^4$ m/m^2).

Computed tomography (CT) is used to determine inhomogeneities arising from local differences in density. It is applicable to a range of ceramics and minerals and is particularly useful for identifying defects in single crystals. The sample is placed on an automated stage that rotates as a series of X-ray images (radiographs) are captured (much like a medical CT scan except that details as small as a few tens of microns can be resolved even in dense samples). A computer then processes the X-ray images and creates a three-dimensional (3D) reconstruction of the sample. Areas of lower density, such as cracks and voids, appear as darker contrast against a lighter background. Figure 10.4 shows density variations in the core of an Nd-doped YVO_4 sample.

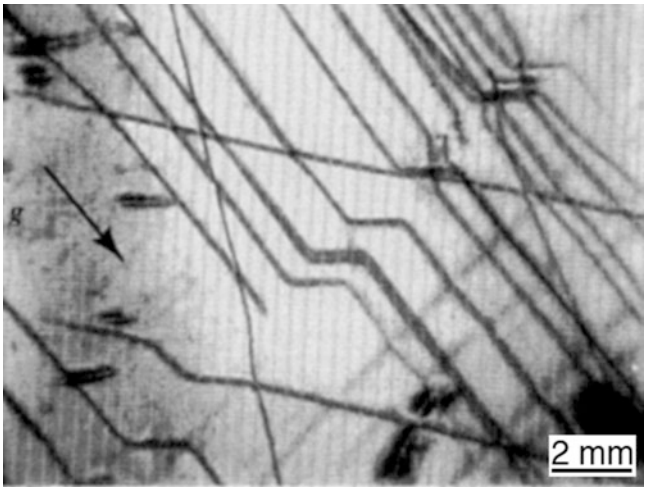

FIGURE 10.3. X-ray topography image showing dislocations in potassium dihydrogen phosphate (KDP) imaged using a 022 reflection.

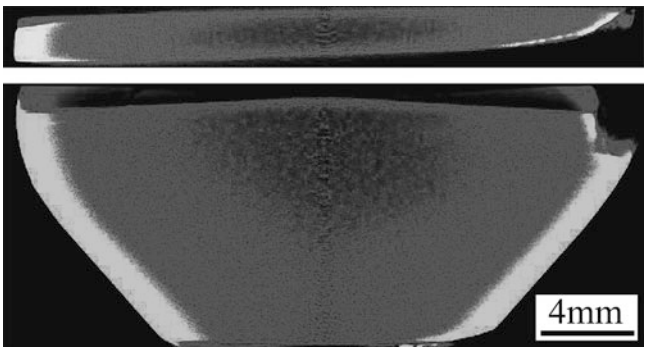

FIGURE 10.4. High-resolution X-ray computed tomography images from the top and side of the same sample.

10.4 IMAGING IN THE SEM

The basic layout of the SEM is shown in Figure 10.5. The SEM can have two imaging detectors: one for secondary electrons (SEs) and one for higher-energy backscattered electrons (BSEs). The SEM typically has a resolution in secondary-electron (SE) mode of 0.7 nm (at 25 kV) and 2.5 nm in BSE mode at 5 kV. In addition to the excellent spatial resolution, the other great advantage of the SEM is that it has a much greater depth of field than the VLM (the depth of field is several millimeters), so the images appear more three-dimensional. The physical reason for this is that the electron beam is very narrow.

The SEs are low-energy electrons, so they are very sensitive to surface topology. Figure 10.6 shows an example of an SE image, illustrating the excellent depth of field. BSEs are higher-energy electrons and are sensitive to the atomic number of the scattering atom. Hence, the intensity of the BSE signal depends on a combination of the average atomic number and density of the ceramic. As the kilovoltage is reduced, the scattering volume becomes more localized close to the surface of the sample. (The

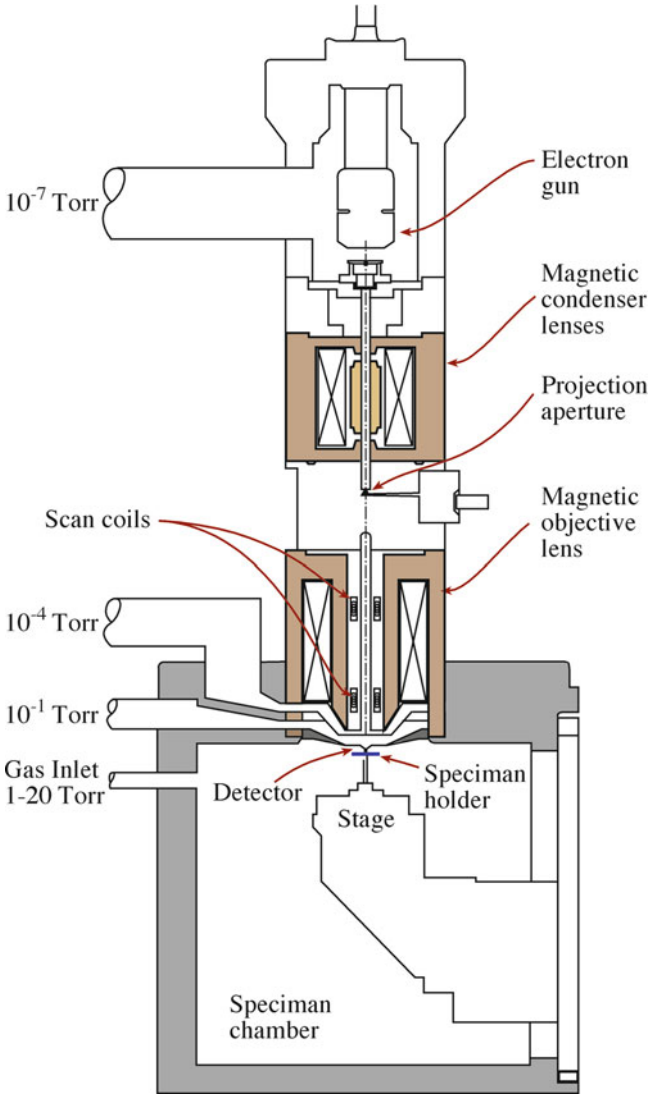

FIGURE 10.5. Schematic of an SEM showing examples of pressures used.

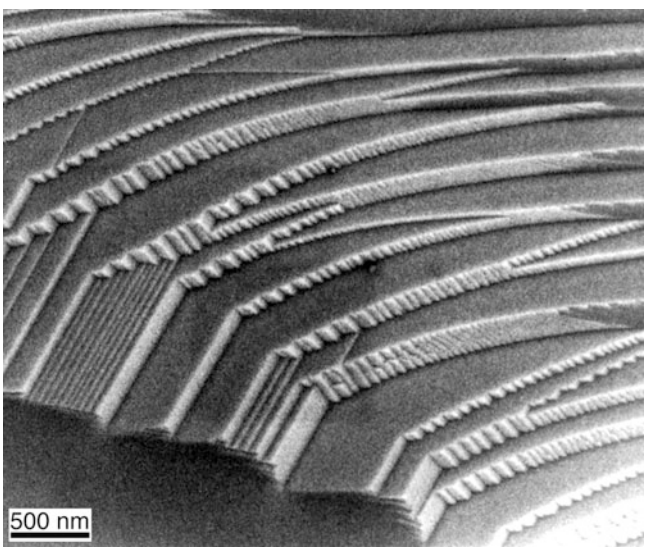

FIGURE 10.6. Secondary electron (SE) image shows steps on an alumina surface.

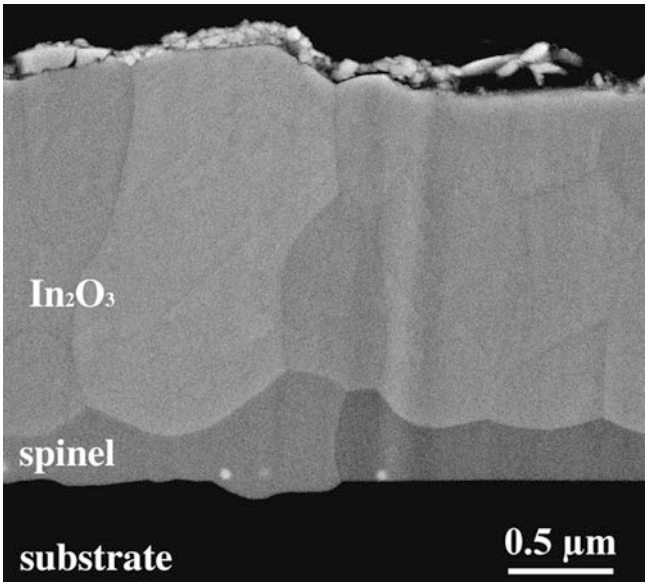

FIGURE 10.7. Backscattered electron (BSE) microscopy shows different contrast from different materials in an MgO/In_2O_3 reaction couple.

BSE electrons penetrate farther into the sample and have farther to come out after being scattered.) Hence, the BSE image can give excellent mass-discrimination even at low voltages. In Figure 10.7 the three regions correspond to three different layers in a reaction couple. The MgO substrate is darkest, In_2O_3 is lightest, and the spinel, $MgIn_2O_4$, is intermediate. The very bright regions are Pt nanoparticles.

Charging in the SEM is usually avoided by coating the specimen (e.g., with a 1-nm layer of Pt). Working at lower accelerating voltages can also reduce charging effects, but then you compromise on the resolution; electron lenses work better at higher resolutions. In low-voltage SEM imaging, you are trying to balance the electrons emitted as the specimen is irradiated, with the charge building up on the specimen. Another way to avoid applying a conductive coating is to use an environmental or low-vacuum SEM. Then, the charging of the specimen is essential, grounded by the gas in the chamber. Variations in the SEM are summarized in Table 10.3.

Environmental SEMs allow operation at pressures of several Torr (0.1–20 Torr) in the sample chamber and at temperatures >1,000°C. In addition to being able to examine insulators, it is also possible to follow dynamic processes such as drying of cement and crystallization.

10.5 IMAGING IN THE TEM

Figure 10.8 shows a state-of-the-art TEM with a field emission source. The key requirement for using TEM is that we require the sample to be very thin (usually ≤200 nm), so the technique is destructive and specimen preparation can be-time consuming. The benefits, however, are significant. Because of the large range of signals generated by the incident electron beam (Figure 10.9), a TEM allows full characterization of a sample at high resolution. The conventional imaging modes in a TEM

TABLE 10.3 Comparison Summary of Signals Used in SEM

Signal	*Energy*	*Source*	*Use*
Secondary electrons	~5 eV	Loosely bound electrons scattered from surface	Main signal for image formation
Backscattered electrons	Energies up to incident beam energy	Beam electrons scattered back after collision	Atomic number contrast, channeling patterns, magnetic contrast
Characteristic X-rays	Discrete values for each element	Interband transitions usually involving K and L	Chemical analysis
Light (cathodoluminescence)	UV, visible, IR	Interband transitions between higher energy levels	Imaging dislocations in semiconductors

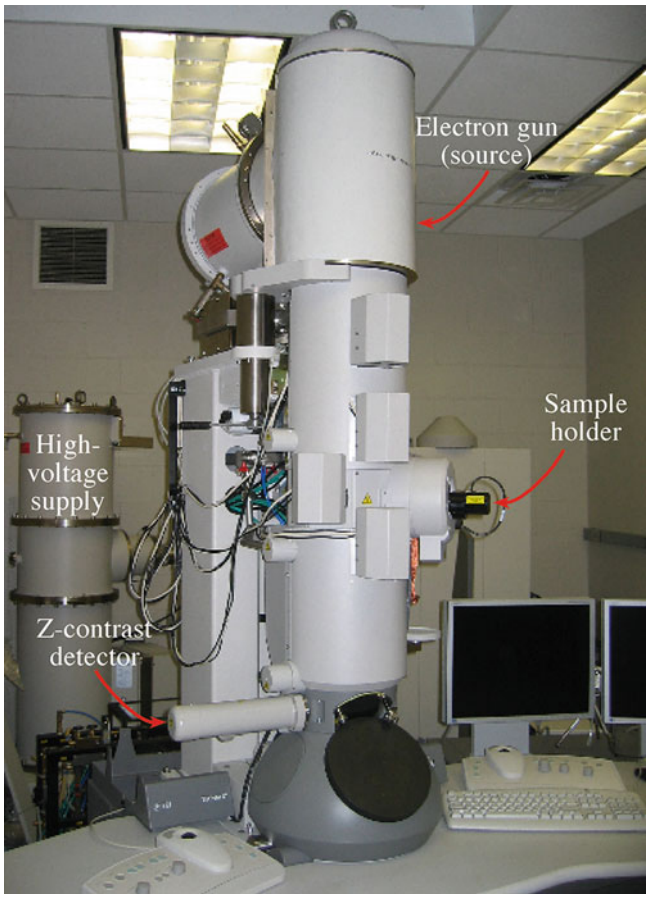

FIGURE 10.8. A TEM with key features labeled.

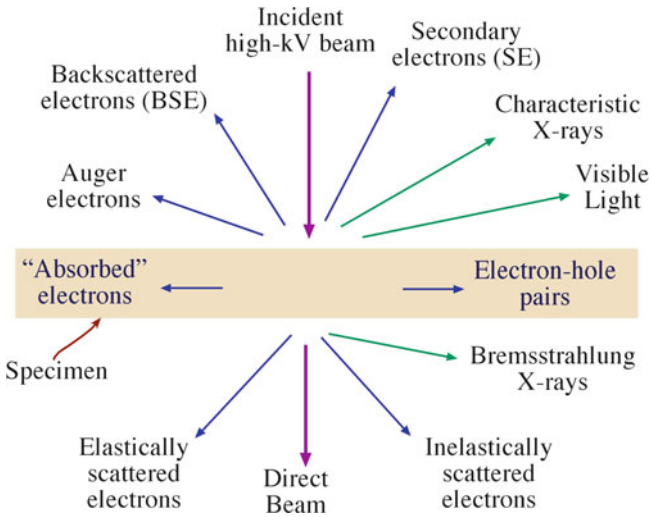

FIGURE 10.9. Signals produced in a TEM.

are bright-field (BF) and dark-field (DF) imaging. In BF imaging, the image is formed using only the direct beam. An aperture (the objective aperture) is used to exclude all the diffracted electrons from contributing to the image. In DF imaging, the image is formed from one of the elastically scattered beams, and the objective aperture blocks the direct beam and all the other scattered electrons. The BF image in Figure 10.10a shows a thick particle of NiO sitting on a thin film of Al_2O_3; the different gray levels in the films correspond to different thicknesses in the Al_2O_3 film. The DF image in Figure 10.10b shows the same region after reacting the two oxides at high temperature; by using a reflection that is excited only by the spinel product, we can see exactly where the spinel has formed.

The resolution of a TEM is determined by the energy of the electrons (controlled by the accelerating voltage), the thickness of the specimen (we want to avoid multiple scattering within the sample), the distance between the sample and the objective lens, and the inherent quality of the lens (defined by its spherical aberration coefficient). Figure 10.11, an image of $SrTiO_3$, shows variations in the oxygen occupancy. In 2012, the best high-resolution TEM has a resolution of 0.05nm. For nanotechnology, high-resolution (HR) TEM is an essential tool. An example is its use in studying crystals of KI grown in a boron nitride nanotube, as shown in Figure 10.12.

RESOLUTION
The higher the resolution the smaller the features we can resolve.

10.6 SCANNING-PROBE MICROSCOPY

The topic of scanned probe microscopy includes several techniques that grew out of the development of scanning tunneling microscopy (STM) (which shared the Nobel Prize in 1986). The basic principle is that the tip of the probe determines the resolution of the image, as shown in Figure 10.13. STM has been used to study the atomic

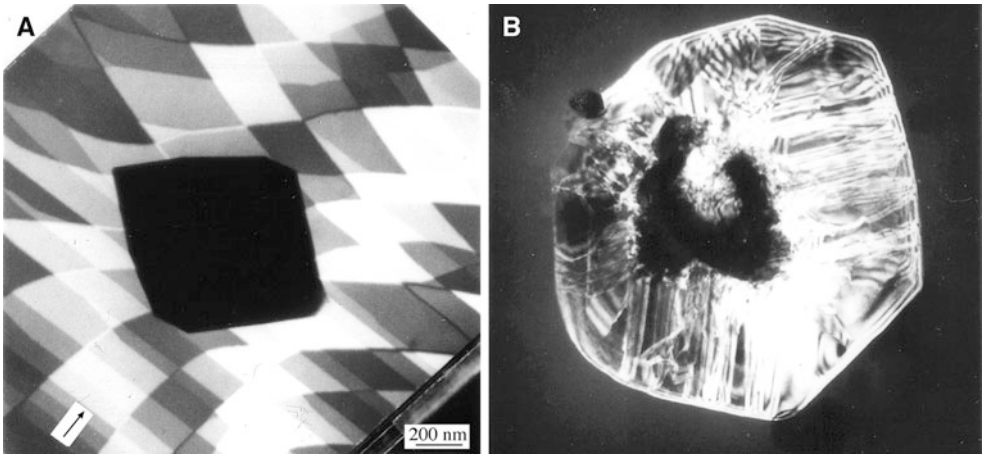

FIGURE 10.10. Bright-field (A) and dark-field (B) microscopy (using a spinel reflection) of a particle of NiO on a film of Al_2O_3 before and after reaction.

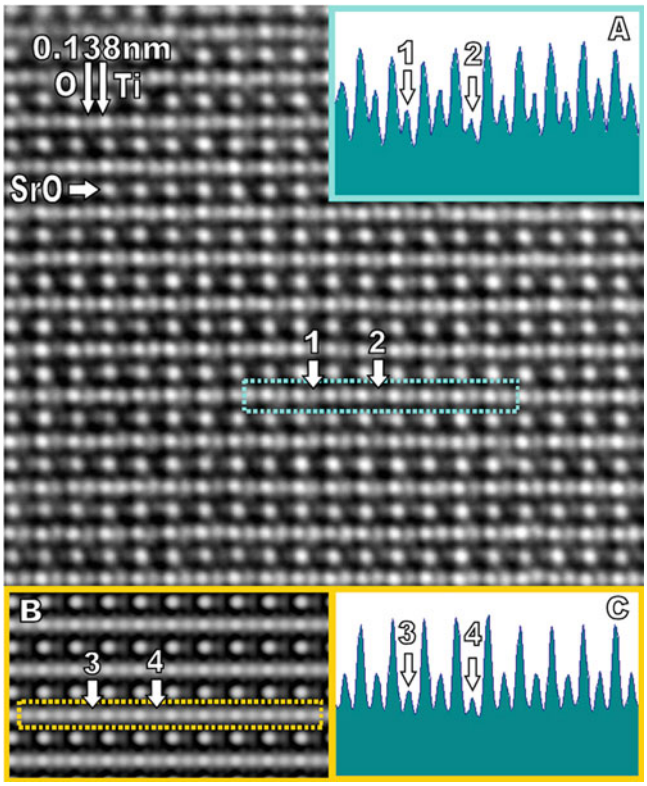

FIGURE 10.11. High-resolution (HR) TEM image of the structure of $SrTiO_3$.

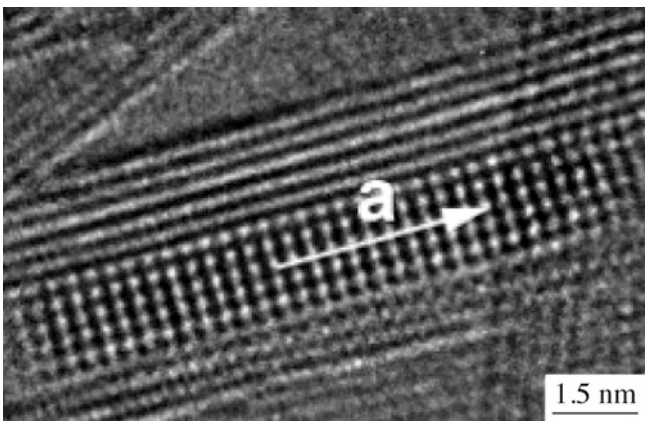

FIGURE 10.12. HRTEM image of a BN nanotube partly loaded with a crystal of KI.

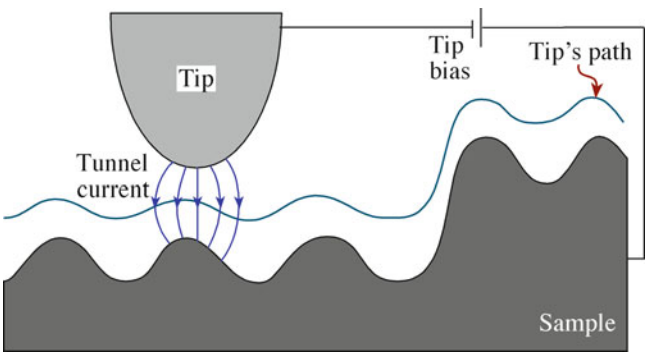

FIGURE 10.13. Tip–sample interaction seen by scanning tunneling microscopy (STM). The tip does not make physical contact with the sample.

structure of ceramic surfaces. Figure 10.14 shows the reconstructed (110) surface of TiO_2. In addition to STM, there are now several other types of scanned probe microscopy. The most widely used is atomic-force microscopy (AFM), illustrated in Figure 10.15. AFM is extensively used to study the surfaces of nonconducting oxides. AFM images at low and high magnification, respectively, are shown in Figure 10.16. The lines are straight single steps (0.4 nm high) on the surface of (111) spinel; the high-magnification image shows that the origins of the steps are a pair of dislocations emerging at the surface. A nano-scale indenter can be attached to the AFM, making it into an indenter with integrated imaging. Table 10.4 summarizes the common operating modes of the AFM.

AFM AND STM 'IMAGE' ATOMS

Both AFM and STM provide atomic resolution, meaning we can resolve individual atoms.

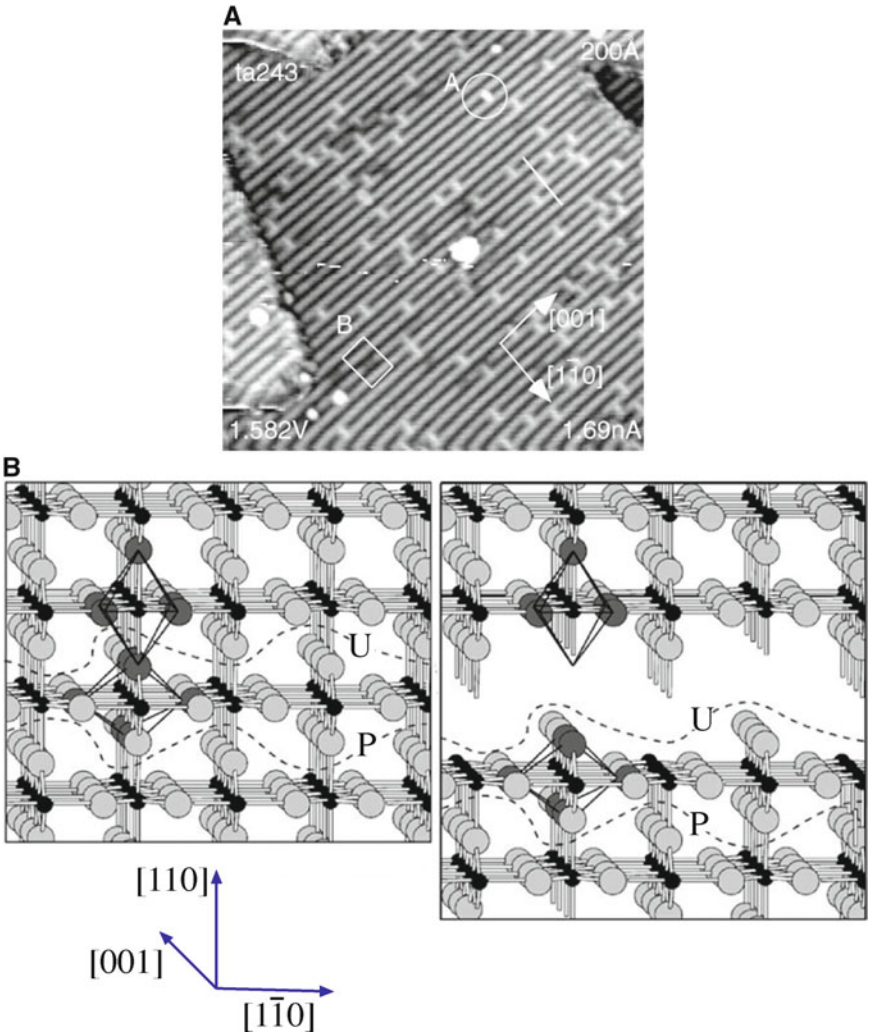

FIGURE 10.14. STM image of the (110) surface of TiO_2. The features labeled "A" have been assigned as oxygen vacancies; the features labeled "B" have not been identified. The model shows how such a surface can be formed. The dashed lines indicate where the 'break' can occur. Large spheres are the O anions.

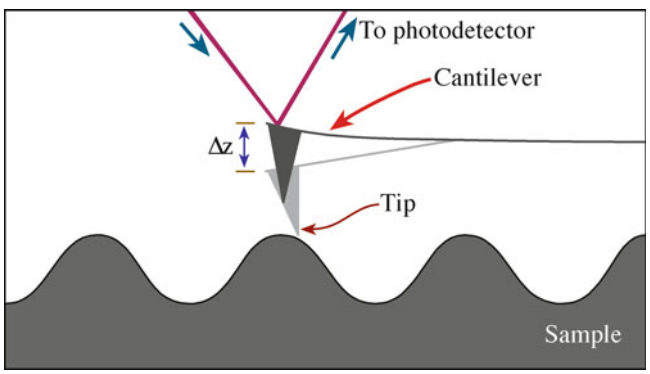

FIGURE 10.15. Tip–sample interaction shown by atomic-force microscopy (AFM) using a cantilever system.

10.7 SCATTERING AND DIFFRACTION TECHNIQUES

The fundamental idea is that we scatter particles or waves from the constituent atoms in the sample. If the waves interfere constructively, we have diffraction, which implies that the sample is at least partly crystalline. If the sample is not crystalline, we may still learn about the distribution of the atoms from the radial distribution function (RDF). The process of scattering generally implies particles; diffraction generally suggests Bragg diffraction or constructive interference of waves.

We can summarize some techniques in diffraction and scattering (of photons, electrons, neutrons, for example).

Photon scattering	Raman and Fourier transform infrared (FTIR) are well known techniques for the chemist and increasingly important in ceramics
Electron diffraction	Selected-area diffraction (SAD) in the TEM
	Convergent-beam electron diffraction (CBED) in the TEM
	Electron-beam backscattering diffraction (EBSD) in the SEM
	Reflection high-energy electron diffraction (RHEED) in UHV for surfaces
Ion scattering	Rutherford backscattering spectrometry (RBS)

(continued)

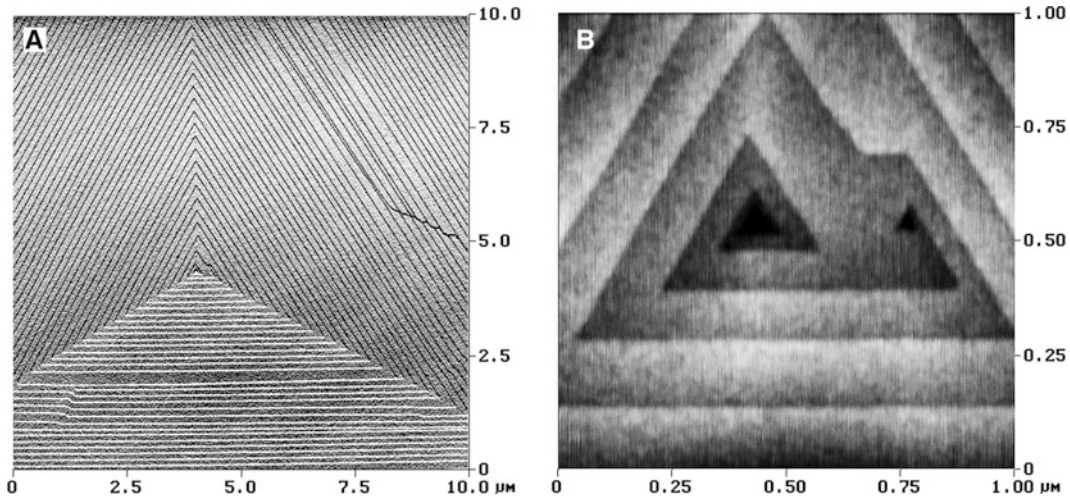

FIGURE 10.16. AFM image showing long (up to 10 μm) straight steps on the surface of an Mg–Al spinel. The steps are 0.4 nm high. The lower image shows the central region at higher magnification.

X-ray diffraction	Powder diffraction for statistical determination of lattice spacings
	Laue back-reflection for orienting single crystals
Neutron scattering	Small-angle scattering in a range of environments

TABLE 10.4 Modes of Operating the Atomic-Force Microscope

Mode of operation	*Force of interaction*
Contact mode	Strong (repulsive); constant force or constant distance
Noncontact mode	Weak (attractive); vibrating probe
Intermittent contact mode	Strong (repulsive); vibrating probe
Lateral force mode	Frictional forces exert a torque on the scanning cantilever
Magnetic force	Magnetic field of the surface is imaged
Thermal scanning	Variation in thermal conductivity is imaged

Electrons interact most strongly with the sample, so for transmission the specimen must be thin and in a vacuum. Neutrons are at the other extreme but can be used only in dedicated (usually national) facilities because they require radioactive sources.

We use diffraction in the TEM to study the crystallography of the interfaces and characterize other crystal defects. Bragg made the first direct determination of a crystal structure using X-ray diffraction (XRD). XRD is still generally the most accurate method for characterizing crystal symmetry, provided the sample is large enough and can be isolated. However, XRD does not provide a high spatial resolution because the beam diameter is typically 1 mm, although with a rotating anode generator it may be 0.1 mm; and with a synchrotron $\leq$1 μm is possible.

10.8 PHOTON SCATTERING

Electromagnetic spectroscopy involves the interaction of electromagnetic waves and matter. We can use all regions of the electromagnetic spectrum, and each gives specific information about a material. Table 10.5 provides a summary, and succeeding sections deal with each of the methods in a little more detail with specific application to ceramics. Once again, to really understand each of the methods you need to read a specialist text.

10.9 RAMAN AND IR SPECTROSCOPY

Raman and IR spectroscopy both involve the scattering of light. In IR spectroscopy, the light is polychromatic and couples to vibrational modes in the solid through dipole moments, which are associated with the vibration. These vibrational modes cause a dip in the transmission spectra or a peak in the absorption spectra. The IR range is 0.78–1,000 μm (12,820–10 cm^{-1}). The region where most fundamental vibrational modes occur, which is the most useful for materials characterization, is 2.5–25 μm (4,000–400 cm^{-1}). This is sometimes called the mid-IR region. The light source is a heated ceramic (usually a conducting ceramic or a wire heater coated with ceramic) that emits a range of frequencies.

- Spectroscopy: the art of using a spectroscope
- Spectrometry: the act of using a spectroscope

An important variant is the FTIR spectrometer. The main advantages of FTIR are that it is much quicker because it measures all the frequencies simultaneously, and it is more sensitive than dispersive IR spectrometers.

TABLE 10.5 Electromagnetic Spectroscopy

Energy

E [eV] (× 96,485 from J/mol)	10^{-7}	10^{-5}	10^{-2}	10^{-1}	10^{1}	10^{-3}	$>10^{3}$
T (K)	1.16×10^{-3}	1.16×10^{-1}	1.16×10^{2}	1.16×10^{3}	1.16×10^{5}	1.16×10^{7}	$>10^{7}$
ν (Hz)	2.4×10^{-7}	2.4×10^{9}	2.4×10^{12}	2.4×10^{13}	2.4×10^{15}	2.4×10^{17}	$>10^{17}$
λ (cm)	1.24×10^{3}	1.24×10^{1}	1.24×10^{-2}	1.24×10^{-3}	1.24×10^{-5}	1.24×10^{-7}	$>10^{-7}$
Radiation	Radio	Micro	IR	VIS	UV	X	γ
Atomic subsystem transitions	Nuclear spins	Electron spins	Rotation vibration	Outer shell electrons		Inner shell electrons	Nuclei
Primary quantity measured	Local interactions (magnetic, electric field gradient)		Atomic molecular potentials	Energy levels		Energy levels	Energy levels
Kinetic parameter detected	Diffusional atomic motions		Vibrational frequencies	Macroscopic, real time kinetic coefficients, point defect concentrations			
Effects on reactivity			Transport activation by heat	Photochemistry		Radiation chemistry	
Characteristic sample dimension [cm]	10^{-1}–10^{0}	10^{-2}–10^{-1}	*ca.* 10^{0}	10^{-4}–10^{0}		10^{-2} (A1, 10^{4} eV)	10^{-3} (Fe(MS)) 10^{-1} (In(PAC))
Examples of methods	NMR	ESR	Raman	Absorption spectroscopy		XAS	Mössbauer, PAC

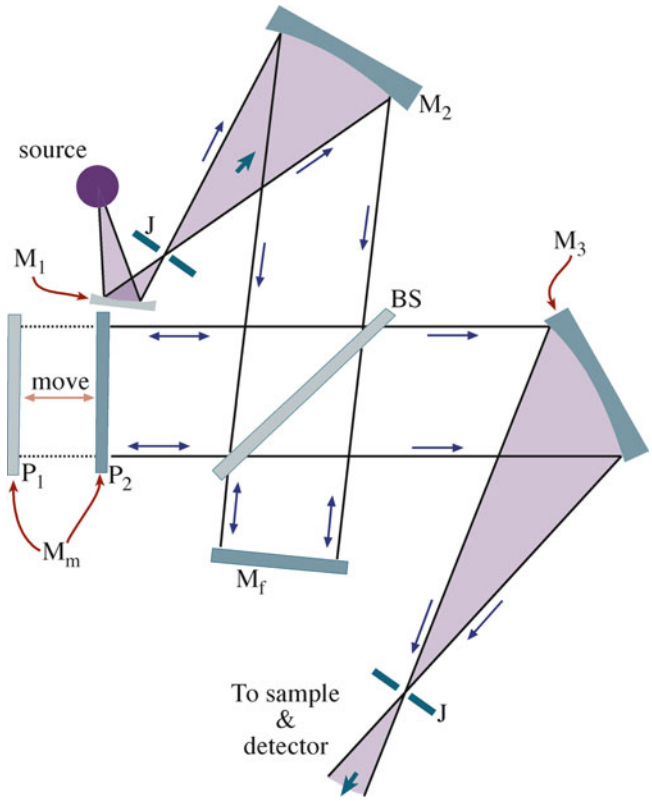

FIGURE 10.17. Arrangement of mirrors and ray paths in Fourier transform infrared (FTIR) microscopy.

Cryo-cooled HgCdTe detectors are used for weak signals or high resolution.

The key component of an FTIR is the interferometer, which can be understood by considering the Michelson interferometer shown in Figure 10.17. A parallel beam directed from the source is split at B_s so 50% of the light is transmitted and reflected back by mirror M_F, and the rest is reflected at B_s and then again at M_M. The beams recombine at B_s. The recombined beam shows constructive or destructive interference depending on the difference in the path lengths B_s to M_F and B_s to M_M. As M_M is moved smoothly toward or away from B_s the detector sees a signal altering in intensity. If the recombined beam from B_s is passed through a sample before reaching the detector, sample absorptions show up as gaps in the frequency distribution. The complex intensity distribution received by the detector is Fourier transformed by a computer to produce an absorption spectrum.

Infrared spectra are output in the form of plots of intensity (percent transmittance, %T, or absorbance (A) versus either energy (in joules), frequency (in hertz), wavelength (in micrometers), or wavenumber (per centimeter)). The use of wavenumber is preferred, but some of the standard reference sources of IR spectra use wavelength. FTIR can be used to determine the oxygen content in silicon. The Si–O stretching band occurs at 1,105 cm^{-1}, and from the peak intensity the oxygen concentration can be determined using ASTM standard F 121. The FTIR absorption spectra in Figure 10.18 are from $Li_{0.1}Mn_2O_4$ after heating for 8 h at 250°C and 18 h at 300°C. These FTIR readily distinguishes them from the binary oxide MnO_2.

In Raman spectroscopy, the light is nearly monochromatic and is usually in the visible range. The light source is a laser (e.g., a 50 mW 785 nm diode laser). Raman spectroscopy has become a routine tool for exploring the structure and chemical properties of materials. It can provide more information than IR spectroscopy. There are three types of signal in a typical Raman experiment, as illustrated in Figure 10.19.

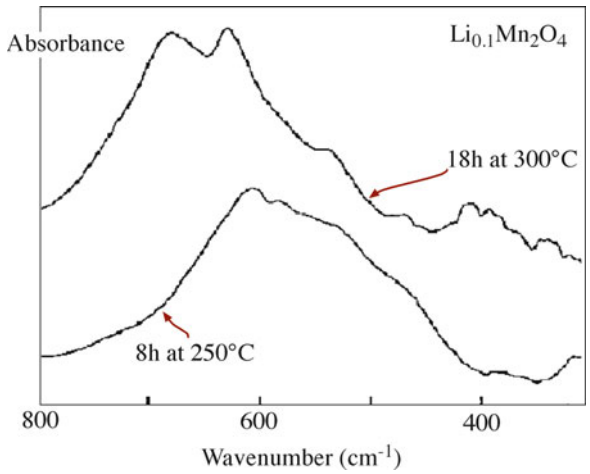

FIGURE 10.18. FTIR absorption spectra from $Li_xMn_2O_4$ insertion electrodes after different heat treatments.

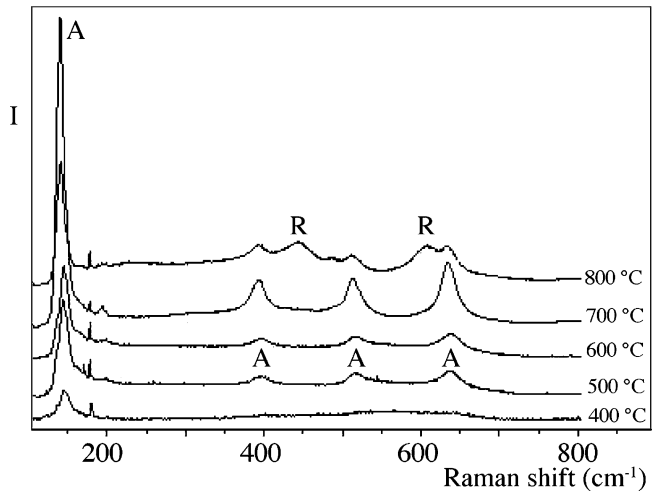

FIGURE 10.20. Example of Raman spectra from a TiO_2 film heated to different temperatures. *R* rutile, *A* anatase.

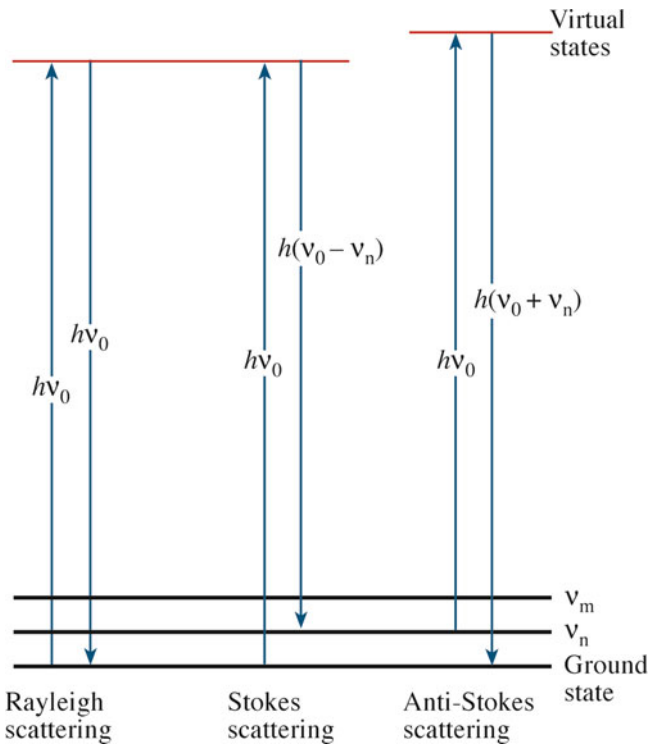

FIGURE 10.19. Transitions occurring in Raman spectroscopy.

The scattering process can be anti-Stokes, Rayleigh, or Stokes. We are then interested in measuring the intensity and the Raman shift.

In *Rayleigh scattering*, a molecule is excited by the incident photon to a virtual energy level. This energy level is caused by distortion of the electron distribution of a covalent bound. The molecule returns to the vibrational ground state by emitting the same energy, E_0 ($E_0 = h\nu_0$). Rayleigh scattering is an elastic process.

Vibrational excitations can be created that cause a decrease in the frequency (i.e., in energy) of the scattered light; or they can be annihilated, which causes an increase. The decrease in frequency is called *Stokes scattering*, whereas the increase is *anti-Stokes scattering*. Stokes scattering is the normal Raman effect, and Raman spectroscopy generally uses Stokes radiation.

Figure 10.20 shows a typical Raman spectrum. It is a plot of scattered light intensity as a function of frequency shift (Raman shift, per centimeter) in which the shift is calculated relative to the laser line frequency that is assigned as zero. The material is TiO_2 films prepared by the sol–gel technique that have been annealed at temperatures between 400°C and 800°C. The features in the spectra only correspond to anatase until the film reaches 800°C. At this temperature, a mixed anatase-rutile phase is seen; the pure rutile phase is obtained only at 900°C.

There are increasing applications for Raman spectroscopy. One application is its use in the identification of different pigments in the characterization of historical artifacts. Table 10.6 lists blue pigments used on or before about 1850 that have been identified by Raman spectroscopy.

Variations in Raman spectroscopy include the following:

Laser Raman Microprobe: Allows information to be collected from small samples via the use of a VLM, which allows the region to be selected from which the Raman spectrum is obtained.

Surface-Enhanced Raman Scattering (SERS): For examining surfaces, oxidation, catalysis, and thin films.

Residual Stress Measurement: Scattering depends on local stress, which can be probed in regions as small as 0.7 μm in diameter by Raman spectroscopy.

TABLE 10.6 Blue Pigments Identified by Raman Spectroscopy

Name	*Composition*	*Band wavenumbers, cm^{-1} and relative intensities*	*Excitation λ and power*	*Notes and date*
Azurite	Basic copper(II) carbonate $2CuCO_3{\cdot}Cu(OH)_2$	145w; 180w; 250 m; 284w; 335w; 403vs; 545w; 746w(sh); 767 m; 839 m; 940w; 1,098 m; 1,432 m; 1,459w; 1,580 m; 1623vw	514.5 nm 2 mW	Mineral
Cerulean blue	Cobalt(II) stannate $CoO{\cdot}nSnO_2$	495 m(sh); 532 s; 674vs	514.5 nm 4 mW	1,821
Cobalt blue	Cobalt(II)-doped alumina glass, $CoO{\cdot}Al_2O_3$	203vs; 512vs	514.5 nm 4 mW	1,775
Egyptian blue	Calcium copper(II) silicate, $CaCuSi_4O_{10}$	114 m; 137 m; 200w; 230w; 358 m; 377 m; 430vs; 475 m(sh); 571w; 597vw; 762w; 789w; 992w; 1,012w; 1,040w; 1,086 s	514.5 nm 4 mW	3,000 BC. Also known as cuprorivaite
Lazurite	S3- & S2- in a sodium alumino-silicate matrix $Na_8[Al_6Si_6O_{24}]Sn$	258w; 548vs; 822w; 1,096 m	514.5 nm 4 mW	Mineral (*Lapis lazuli*). Synthetic c.1828 = ultramarine
Posnjakite	Basic copper(II) sulfate $CuSO_4{\cdot}3Cu(OH)_2{\cdot}H_2O$	135vw; 208vw; 278vw; 327vw; 467w; 612w; 983vs; 1092vw; 1139vw	632.8 nm 3 mW	Mineral
Prussian Blue	Iron(III) hexa-cyanoferrate (II) $Fe_4[Fe(CN)_6]_3{\cdot}14\text{-}16H_2O$	282vw; 538vw; 2,102 m; 2154vs	514.5 nm 2 mW	1,704. Earliest synthetic modern
Smalt	Cobalt(II) silicate $CoO{\cdot}nSiO_2$	462vs; 917 m	514.5 nm 2 mW	~1,500

10.10 NMR SPECTROSCOPY AND SPECTROMETRY

Just as each electron has a spin of ±½, each neutron and proton in the nucleus also has a spin, I, of ½. These spins combine, so that each atom has a total nuclear spin of 0, ½, or 1, and an angular momentum P_I, given by

$$P_I = (h/2\pi)\sqrt{[I(I+1)]} \qquad (10.1)$$

The principle of nuclear magnetic resonance (NMR) is that the probing beam is tuned until it couples with the natural angular momentum of the nucleus, which then resonates and emits energy that is measured. The specific quantities depend on the atom that is resonating. The precise value of the energy involved changes slightly if the electron distribution around the resonating nucleus changes, as is the case when the atom is bonded to other atoms; we use NMR to examine this chemical shift. NMR thus probes the bonding of individual atoms. Clearly, for the technique to be applicable the nucleus must have a nonzero total nuclear spin. Fortunately, there are many isotopes, such as ^{29}Si, ^{27}Al, ^{11}B, which are important for ceramics that are suitable. Notice that we have to use ^{29}Si ($I = ½$) not the more abundant ^{28}Si.

When a nucleus that has a nonzero P_I is subjected to a magnetic field of strength H, the energy levels are split into $2I + 1$ different values. The energy separation of the different levels is

$$\Delta E = \gamma Hh/2\pi \qquad (10.2)$$

where γ is called the gyromagnetic ratio of the nucleus. If we then subject this nucleus to electromagnetic radiation and adjust the frequency, ν, to be ν_0 so that it has the same energy ΔE (now $h\nu_0$), the quanta of radiation can be absorbed as transitions between the different nuclear spin energy levels occur. We then detect the NMR absorption in the spectrum as a single peak corresponding to ν_0, which is broadened because the atoms interact differently depending on their neighbors.

There are two particularly important interactions to consider.

- The dipole interaction is the interaction between adjacent nuclei and the one you are probing (such as an interaction between magnetic dipoles)
- The electrons surrounding the nucleus also move because of the applied magnetic field; this is the chemical shift—electrons determine chemistry

The technique can be carried out using either a continuous wave (CW) or a pulsed spectrometer. Radiofrequency (RF) energy is used to excite the nuclear magnetization. The measurement is the response of the spin system to this excitation. In CW the nuclear magnetization is irradiated at a constant level; the frequency of the irradiation or the magnetic field is then swept across the resonance.

The NMR systems are available in most research universities with a basic system costing from $200,000 up to more than $1,000,000, depending mostly on the desired field strength (1–14 T).

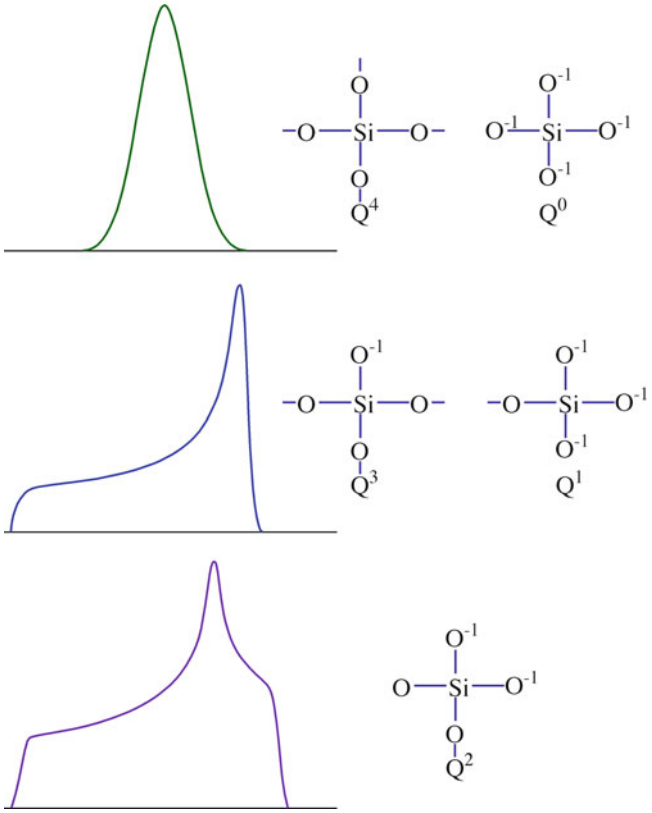

FIGURE 10.21. Nuclear magnetic resonance (NMR) signals from Si.

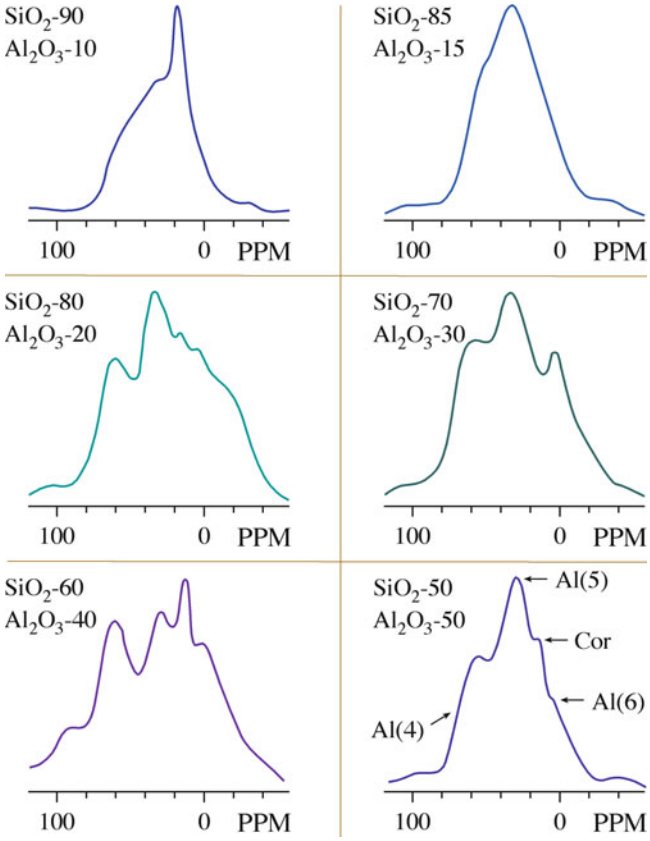

FIGURE 10.22. NMR signals from an Al-Si glass.

The following examples are selected to illustrate why NMR is so valuable for the ceramist. The *x*-axis is in units of parts per million (ppm), which is the chemical shift as a fraction of the applied field or frequency. In Figure 10.21, three NMR powder patterns are shown for silicon in three different chemical environments but where the Si is tetrahedrally coordinated in each case. The differences between the spectra are due to the number of nonbridging oxygen ions that are attached to the Si nucleus being probed: a chemical-shift effect. The value of NMR for studies of silicate glass is obvious.

Figure 10.22 shows a series of NMR spectra from Si–Al glasses. The field used was 11.7 T. The NMR spectra show that not only is the Al present in fourfold, fivefold, and sixfold coordination but there is also undissolved Al_2O_3 present in the glass (denoted "Cor" in the spectra). The chemical shift has been determined using a standard of octahedral ^{27}Al in $AlCl_3$ solution.

10.11 MÖSSBAUER SPECTROSCOPY AND SPECTROMETRY

Mössbauer spectroscopy is specialized but can be invaluable when it is available. The technique relies on the recoil-free emission and resonant absorption of γ rays by nuclei that are bound in the solid state. (If it's not in a solid, the free nucleus recoils and you don't detect a resonance.) To see this resonance, we have to match the energy of the γ-ray emitter to the energy of the absorber (the sample), which means that there are only a small number of elements that can be studied. Two that can be studied are tin and iron. The technique gives information on the bonding and coordination and on the valence (oxidation) state. Because the technique relies on *Z*, it works for particular isotopes, such as ^{57}Fe for iron with ^{57}Co as the radioactive source of γ rays. (Natural Fe contains ~2.19 wt.% ^{57}Fe.)

Figure 10.23 shows a schematic of a Mössbauer spectrometer. The radioactive ^{57}Co source is embedded in a nonmagnetic matrix, which is chosen so as not to affect the sample or to absorb the γ rays too strongly. The system can be calibrated using Fe metal; the six peaks seen in Figure 10.24 correspond to the six transitions expected for ^{57}Fe. The ^{57}Co source has an emission peak at 14.4 keV; the source is moved through a range of velocities using a velocity transducer.

Mössbauer spectra from a series of glasses containing Fe in different oxidation states are shown in Figure 10.25. The differences in the curves are clear; but the analysis needed to determine the percent of Fe in the 2+ state requires extensive calibration of the system. (Notice that peak locations are shown in units of velocity.) The value of the technique is its sensitivity to determining both the oxidation state and the coordination of the Fe ion. Nuclei

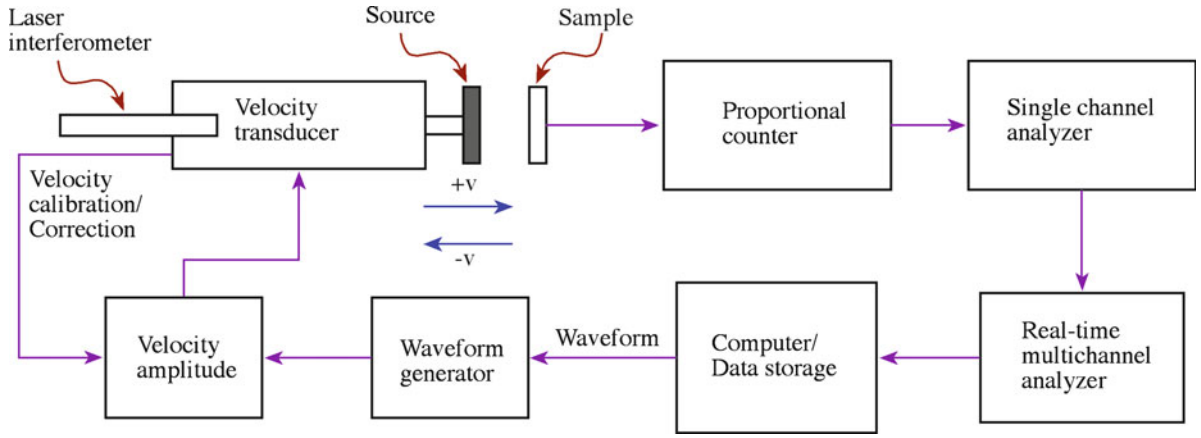

FIGURE 10.23. Setup for Mössbauer spectroscopy.

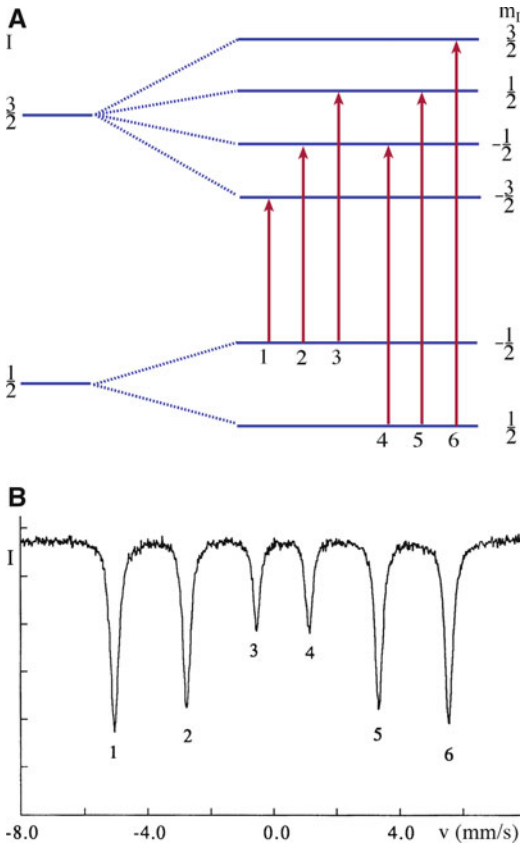

FIGURE 10.24. Transitions in Fe and the resulting Mössbauer spectrum.

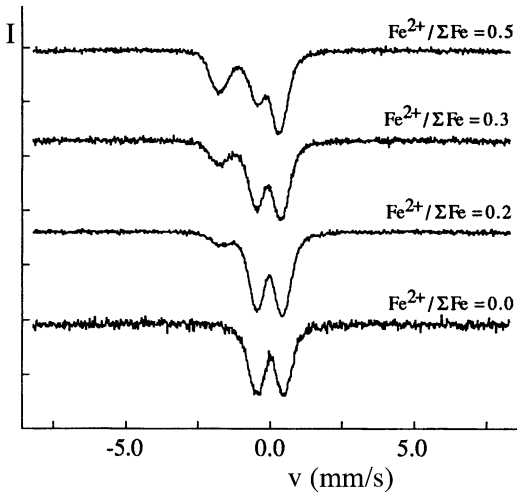

FIGURE 10.25. Mössbauer spectra from glasses containing different concentrations of Fe^{2+}.

in chemical surroundings different from the source do not absorb at the same frequency; this is known as the chemical (or isomer) shift and is the key feature of Mössbauer spectroscopy.

Other isotopes that have been studied are ^{119}Sn (source: metastable ^{119}Sn), ^{121}Sb (source: metastable ^{121}Sb), and ^{151}Eu (source: ^{151}Sm). Table 10.7 lists chemical shifts for tin. It is then quite straightforward to determine the valence state of an unknown tin compound from its Mössbauer spectrum. This type of analysis has been used in studying tin glazes and tin-containing ceramic pigments. It requires quite small amounts of material, typically 50 mg of powder. Bulk materials can also be examined.

TABLE 10.7 Chemical Shift of Some ^{119}Sn Compounds

Valence state	*Electron configuration*	*Chemical shift (mm s^{-1})*
Sn^{4+}	$5s^0 5p^0$	0
Sn (4-covalent)	$5(sp^3)$	2.1
Sn^{2+}	$5s^2 5p^0$	3.7

10.12 DIFFRACTION IN THE EM

The techniques are:

- Selected area diffraction (SAD) in the TEM
- Convergent beam electron diffraction (CBED) in the TEM
- Electron backscattered diffraction (EBSD) in the SEM

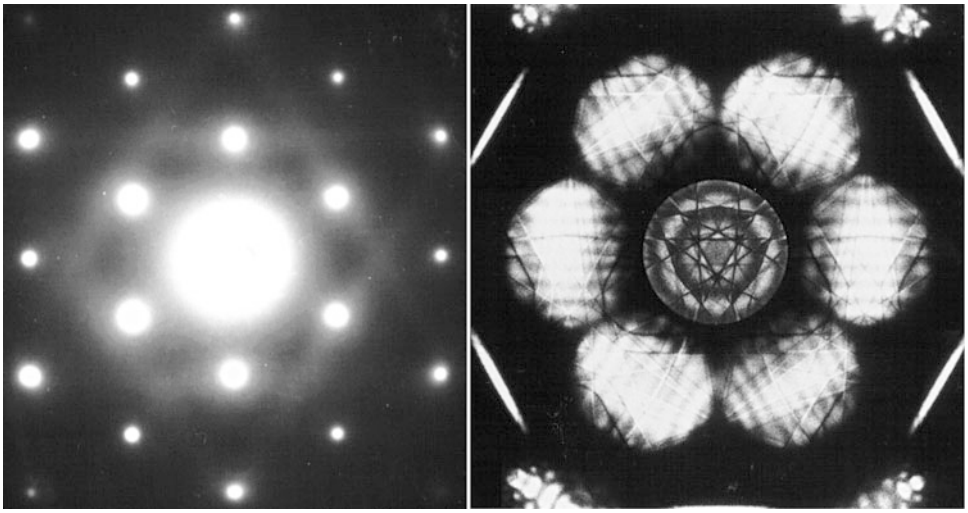

FIGURE 10.26. TEM diffraction patterns obtained using selected-area diffraction (SAD) and convergent-beam electron diffraction (CBED)

Selected-area diffraction involves selecting an area on the sample (actually an image of the area) with an aperture and then looking at the diffracting pattern from that area. The diameter of the area can be as small as 100 nm with a modern machine. In CBED, the diffracting area is selected by focusing the electron beam onto a small area of the sample. The diameter of the area can actually be smaller than the unit cell. Figure 10.26 compares SAD and CBED patterns. From the positions of the spots (in SAD) and the discs (in CBED), we can obtain information about the structure and orientation of our sample. CBED patterns often contain additional, fine structure, which allows determination of symmetry, such as the point group. The value of CBED lies in its ability to provide information on lattice parameters, sample thickness, and local crystallography on a scale of 10 nm or better. We can use the technique to characterize polarity change across antiphase boundaries (APBs) in GaN and AlN, to determine the site occupancy in nickel-titanate spinel and to determine the thickness of a specimen. The latter parameter is used in analyzing the height of steps on surfaces and in quantifying X-ray energy dispersive spectroscopy (XEDS) data.

Diffraction in the SEM can take several forms, but EBSD is now becoming a routine addition to the SEM. The beam penetrates the sample and is backscattered; we can use these electrons to form a BSE image, or we can record the actual diffraction pattern. A schematic of the system is shown in Figure 10.27 together with an example of an EBSD pattern.

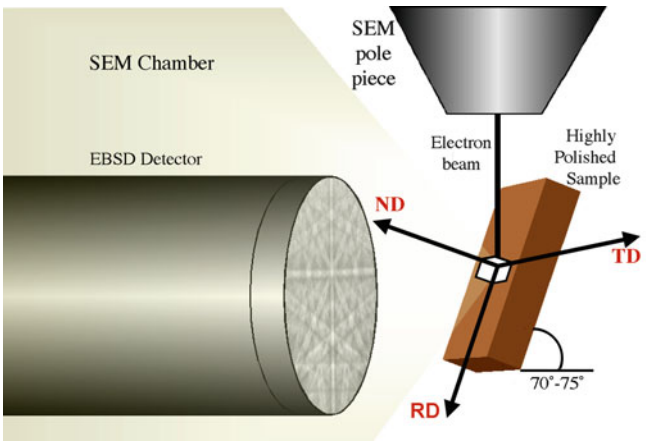

FIGURE 10.27. Formation of an electron-beam backscattering diffraction (EBSD) pattern.

10.13 ION SCATTERING (RBS)

Rutherford backscattering spectrometry again uses ions (a high-energy He beam) to produce the signal but is more akin to electron energy loss spectroscopy (EELS). We analyze the energy of the backscattered ions and thus determine what atoms they interacted with and where those atoms were located in the sample relative to the surface. RBS uses ions (typically 2 MeV helium ions, $^4He^+$) as the scattered particle. We can picture the interaction mechanism as being a collision resembling that between two billiard balls: the incoming ion transfers energy (and momentum) to the ion in the sample, it is detected as it recoils, and its energy is determined (Figure 10.28). The data are provided in the form of a plot of backscattering yield versus energy, and a typical spectrum is shown in Figure 10.29. Computer analysis of the spectrum gives us the types of atoms in a sample, their concentration, and their depth. The depth resolution is about 20 nm. RBS has been widely used in studies of ceramic thin films deposited onto ceramic substrates such as $BaTiO_3$ on MgO.

RBS has poor sensitivity to light elements such as oxygen and nitrogen, which are both important in many ceramics. However, an enhanced oxygen signal can be obtained at an incident energy of 3.045 MeV. RBS is also used to determine

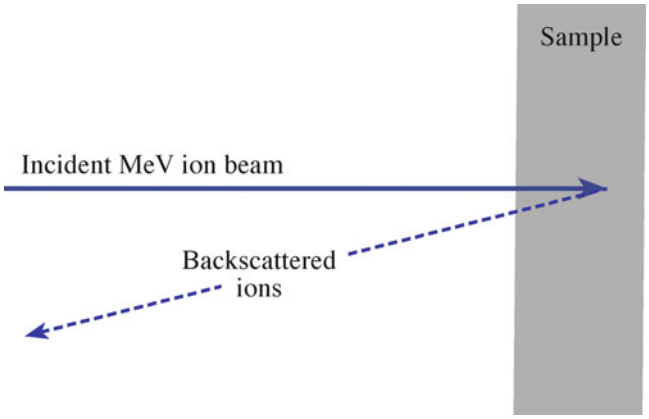

FIGURE 10.28. Backscattering process for Rutherford backscattering spectrometry (RBS). The sample can be tilted to the beam to increase depth resolution.

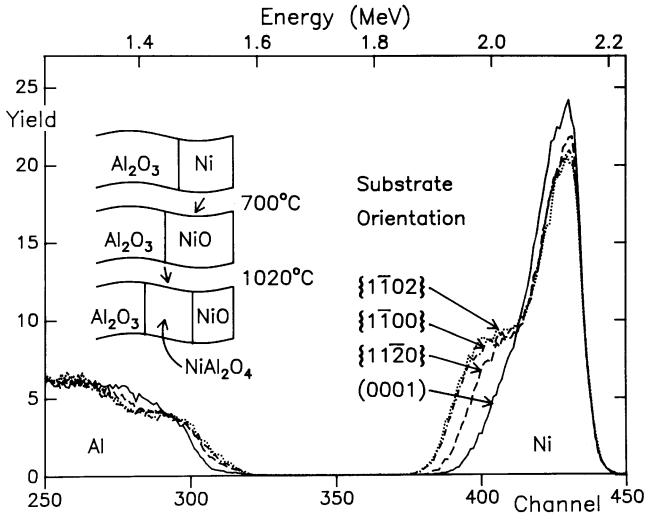

FIGURE 10.29. RBS data sets obtained using a 2.8-MeV beam of He^{2+} ions with the samples tilted 45°. Each sample has been annealed at 700°C for 2 h followed by 1,020°C for 5 h. The Ni peak shows that the extent of the reaction varies with the surface orientation.

the composition of bulk ceramics and impurity profiles in semiconductors (e.g., As distribution in Si).

RBS DETECTION LIMITS

10^{12}–10^{16} atoms/cm^2
1–10 at.% for low-*Z* elements
0–100 ppm for high-*Z* elements

When the ion beam interacts with the sample, it produces particle-induced X-ray emission (PIXE), which is directly analogous to the production of X-rays in the SEM. PIXE has some special advantages over EDS in the SEM in that the background emission is lower, the depth penetration is large, and the sensitivity is high.

10.14 X-RAY DIFFRACTION AND DATABASES

X-ray diffraction is used in several forms depending on the equipment, the sample, and what you want to know. The great advantage of the technique is that a vacuum is not required and that the X-rays can travel through a container before and after interacting with the specimen. For example, the specimen can be heated inside a quartz tube to 1,600°C and examined at temperature. Using a synchrotron, the beam size—and hence the spatial resolution—can be reduced to ~1 μm. A monochromatic beam can be produced such that changes in energy due to absorption can be accurately measured. Table 10.8 lists types of analysis that can be undertaken using X-rays and the specific technique.

One of the most useful sources of information for crystal structure data is the Powder Diffraction File (PDF). The PDF is a collection of single-phase X-ray powder diffraction patterns in the form of tables of interplanar spacings (d) and corresponding relative peak intensities. There are more than 80,000 patterns in the PDF. In the early days the patterns were printed as 3 × 5 in. index cards; and even though everything is now on computer, the files are still referred to as "cards."

Powder XRD this is one of the most widely used techniques to characterize ceramics. The material is in the form of a powder so that the grains will be present in all possible orientations so that all *d* spacings, or θ values, will appear in one pattern. The classical powder pattern was recorded on photographic film. Now the data is

TABLE 10.8 X-ray Diffraction Analysis

Type of analysis	*Method*	*Sample*
Crystal geometry	Moving crystal-spot pattern	Single crystal
	Computer positioned diffractometer	Single crystal
	Solution of *d*-spacing equations	Powder
Arrangement of atoms	Analysis of diffracted intensities	Single crystal
	Refinement of whole pattern	Powder
Symmetry	Moving crystal-spot pattern	Single crystal
	Stationary crystal-spot pattern	Single crystal
Identification of compound	Identification of cell parameters	Single crystal
	Matching of *d*-*I* set	Powder
Crystal orientation	Single-crystal back reflection	Large single crystal
	Texture analysis	Powder compact
Size of crystal	Line broadening	Powder
Magnitude of strain	Line shifts	Powder compact
Amount of phase	Quantitative analysis	Powder
Change of state	Special atmosphere chambers	Single crystal or powder
Crystal perfection	Direct imaging	Single crystal
	Line shape analysis	Powder

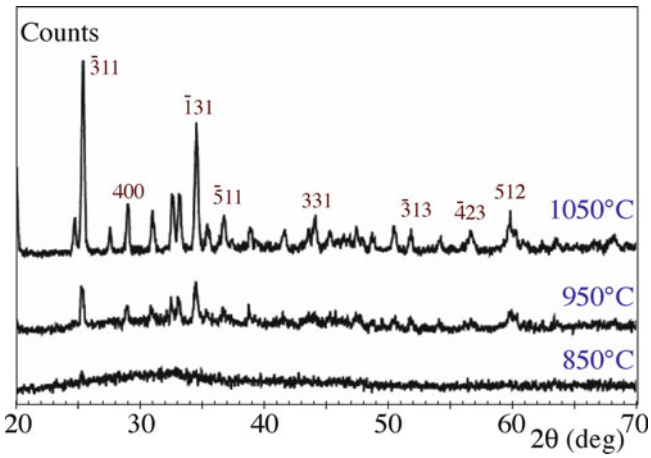

FIGURE 10.30. X-ray diffraction XRD patterns from a mixture of Ca oxide and alumina recorded while heating the sample at different temperatures.

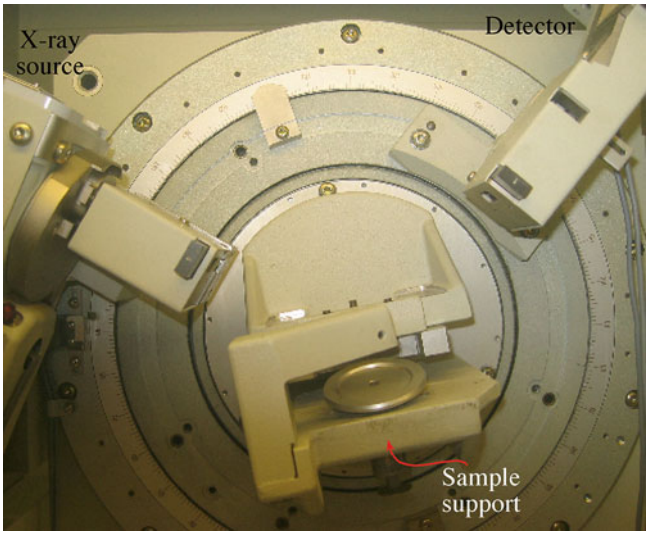

FIGURE 10.31. XRD apparatus shows the location of the source, sample, and detector (Siemens D5005).

in the form of a plot (known as a diffractogram) of counts or intensity versus scattering angle (2θ) as shown in Figure 10.30. A computer that contains the entire PDF is usually used for peak identification. In many examples you will see in the literature phase identification is the extent to which powder XRD is used. This ability alone makes it a powerful and indispensable tool for the ceramist. In a multiphase material the relative amounts of each phase can be determined from the peak areas.

PDF CARD NUMBERS
21–1272 Anatase
29–1360 Brookite

Powder XRD can be used for estimating the sizes of particles. The Scherrer formula says that

$$\Delta\theta \cdot \Delta x = 2\pi \qquad (10.3)$$

where $\Delta\theta$ is the peak width (scattering angle half-width), and Δx is the average particle diameter. The resolution of the diffractometer corresponds to an integral width of 0.32 nm. Notice that the anatase peaks are delta functions at $\Delta\theta = 17.5$ and $\Delta\theta = 33.0$. After correcting for the instrument resolution, the integral widths of the peak are $\Delta\theta = 1.57$ n/m and 1.29 n/m.

Figure 10.31 shows the main components of an X-ray diffractometer. The important features are:

- X-ray source. Often Cu K$\alpha\lambda = 0.154184$ nm because of its high intensity.
- Sample. Usually a powder but can be pressed or sintered. Only a few milligrams are needed.
- Detector. Two main types: proportional detectors use photoelectrons generated in Xe; semiconductor detectors use electron–hole pairs created in p-i-n junctions formed in silicon.

In the θ/2θ X-ray diffractometer, the sample and detector rotate relative to the X-ray source; when one moves through θ, the other moves through 2θ. Alternatively, the sample can be held fixed and the detector and source rotated in opposite directions. The conventional XRD geometry is often referred to as the Bragg-Brentano geometry. Several different geometries and modifications are used for studying ceramics.

Thin-film diffractometer. A glancing angle geometry is used with the sample surface at an angle of 5–10° to the X-ray beam. The basic idea is that the penetration depth of the X-rays is reduced so they are analyzing the surface. Longer wavelength X-rays can be used, which also reduces penetration (switch to a Cr Kα source $\lambda = 0.229100$ nm). Polycrystalline thin films down to a few tens of nanometers thick can be examined.

Microdiffractometer. Collimators as small as 10 μm are used to produce a small X-ray spot size. The geometry of the detection system is also different from a conventional diffractometer in that it uses an annular detector that allows sampling of the entire cone of diffracted radiation.

Hot-stage XRD. The sample is placed inside a quartz furnace tube that can be heated to temperatures up to 1,600°C, often in a range of different atmospheres. The main uses are for studying phase changes and structural transformations as a function of temperature.

Pole figure. Uses a Eulerian goniometer cradle attached to the diffractometer for determination of preferred crystal orientations.

Single-crystal XRD. A single crystal diffractometer allows the orientation of the crystal to be controlled in such a way that every set of planes can be moved into a diffraction condition. The X-rays are usually detected by scintillation. The technique is not as routine as powder XRD, and determination of a crystal structure can take many days or even turn into a thesis.

Laue technique. The diffracted beams produce a pattern consisting of an array of spots. It is used to orient single crystals (with an accuracy of 0.3–1.0°) prior to cutting and polishing.

10.15 NEUTRON SCATTERING

The initial obvious statement is that, overall, neutrons interact with matter even less strongly than do X-rays. Table 10.9 summarizes the differences between the two probes. For both neutrons and X-rays, it is not as easy to direct the beam as it is with electrons or ions. In both cases, the experimental method involves measuring the intensity of the scattered beam as a function of scattering angle.

The obvious question is: Why use them when other particles do interact strongly? Neutrons offer distinct advantages over X-rays and other probes. They have a magnetic moment, so they can detect magnetic ordering. Because they don't interact strongly, they can be used for obtaining bulk information. A major application is residual stress measurement in materials as a function of depth.

Neutrons have been used to study glasses and show a first sharp diffraction peak at low angles. This implies that there is some ordering in the glass. Intentional patterns of voids in glasses give rise to such peaks. Table 10.10 gives a comparison of the parameters for XRD and neutron diffraction.

Neutrons are produced in several ways, but each requires a reactor. Thus neutron diffraction facilities are generally national facilities. There are seven centers for neutron scattering in the United States and about 30 worldwide. A schematic of a neutron diffractometer is shown in Figure 10.32.

TABLE 10.9 Properties of X-rays and Neutrons

Property	*X-ray*	*Neutron*
Wavelength	0.05–0.25 nm	0.01–2.0 nm
Energy	12.4 keV	80 MeV
Velocity	3×10^8 m/s	4×10^3 m/s
Production	X-ray tube	Nuclear reactor
	Synchrotron	Electron linear accelerator pulsed source
		Proton spallation pulsed source
Detection	Photographic film	$^{10}BF_3$ or ^3He proportional counter
	Proportional counter	^6Li scintillation counter
	Scintillation counter	

TABLE 10.10 Scattering of X-rays and Neutrons

Dependence	*X-ray*	*Neutron*
Nonmagnetic atom	Electrons scatter	Nucleus scatters
θ dependence	Depends on θ through $f(\theta)$	Depends on isotropic scattering length $\bar{b}$
Variation with Z	$F(0) = Z$	$\bar{b}$ varies with Z
Phase change on scattering	π	Not always π
Isotope dependence	None	$\bar{b}$ depends on isotope
Anomalous dispersion	Near an absorption edge	Near an absorption resonance
Magnetic atom	Nothing extra	Additional scattering (depends on θ)
Absorption coefficient	Absorption large	Absorption usually small

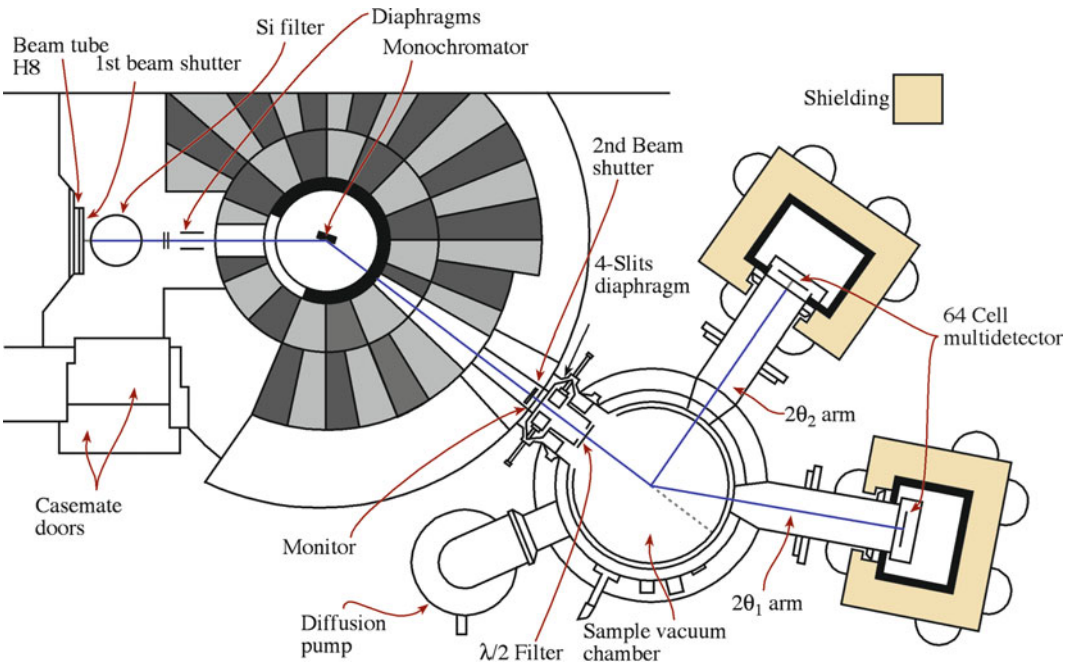

FIGURE 10.32. Schematic of a neutron scattering workstation. The width of the view is 10 s of meters.

10.16 MASS SPECTROMETRY

Mass spectrometry is used to provide qualitative and quantitative chemical analysis. For ceramics we are mainly interested in analyzing solids so a method for ionizing the material is necessary. In spark source mass spectrometry (SSMS) we use a high-voltage spark in a vacuum. The positive ions that are produced are analyzed by the spectrometer based on their mass. For insulating ceramics, the material must be mixed with a conducting powder such as graphite or silver. There are other methods to ionize the sample.

1. Laser ionization MS. Uses a Nd:YAG laser and is ideal for insulators, but it is more qualitative than quantitative because of the absence of standards.
2. Glow discharge ion source. Uses a gas discharge between two electrodes, so the sample must be conductive and formed in the cathode.
3. In secondary ion mass spectroscopy (SIMS) an incident ion beam with energy in the range 4–15 keV, is use to create secondary ions from the sample. SIMS provides high-resolution depth profiles with a detection limit down to 1 ppb.

Scanning ion mass spectroscopy (SIMS) is like SEM but uses ions (usually Ga^+) instead of electrons. Because the ions have more energy, they eject near-surface atoms out of the sample; these atoms are collected and the chemistry of the near-surface area thus determined. By scanning the ion beam we can generate a chemical image of the surface, and by repeating this process (each time ejecting the surface atoms) we can generate a 3D profile of the sample.

10.17 SPECTROMETRY IN THE EM

The chemistry of interfaces can be probed using both XEDS and parallel recording of electron energy-loss spectra (PEELS).

In the earliest studies of solid-state reactions between ceramic oxides, the width of the reaction product produced by bulk diffusion couples was determined by VLM. Using an SEM with a field-emission gun, much more precise EDS profile analysis can be performed and provide chemical analysis at a spatial resolution of ~2 nm. Figure 10.33 shows a typical XEDS spectrum: a plot of counts versus X-ray energy. The X-rays are produced as a result of electron transitions within the atoms in the sample. The transitions, and hence the peaks, are characteristic of specific atoms. A doped silicon crystal is used to detect the X-rays, where they cause the formation of electron–hole pairs. New methods for detecting the X-rays are being developed that use the change in temperature caused by the X-ray; they are known as colorimeters.

The electron microprobe or wavelength dispersive spectrometer (WDS) can provide accurate chemical analysis or chemical profile across the interface. The wavelength of the X-rays emitted when the electron beam interacts with the sample is measured. WDS is more accurate than XEDS but is a serial acquisition, so it is slower. Table 10.11 compares WDS and XEDS.

Electron energy-loss spectroscopy counts the number of electrons that have lost particular quantities of energy when the incident electron beam passes through the TEM specimen. The energy loss can occur by interactions with different components of the structure (phonons and plasmons) or by the beam exciting core electrons to a different energy state. The EELS spectrum thus contains

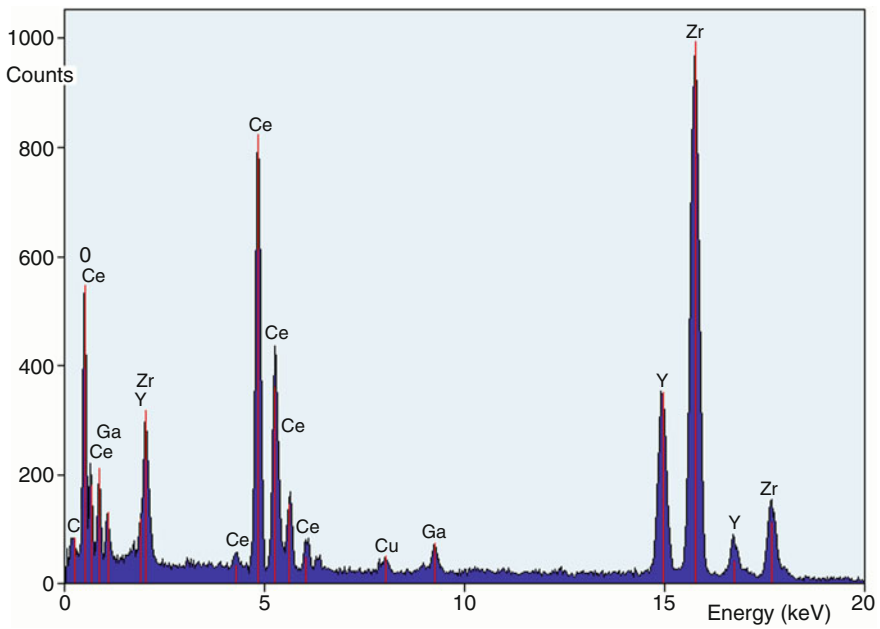

FIGURE 10.33. Example of an XEDS from a sample containing CeO_2 and YSZ in the range up to 20 keV.

TABLE 10.11 Comparison of WDS and XEDS

Factor	*WDS*	*XEDS*	*Reason for difference*
Time for complete spectrum (min.)	25–100	0.5–5.0	(1) Collection efficiency (2) XEDS measures whole spectrum simultaneously
Count rate on one peak (cps/nA)	1,000	10,000	Collection efficiency
Peak/background ratio	1,000	50	XEDS collects spurious X-rays and has high inherent noise
Maximum count rate (cps)	100,000	30,000	XEDS counts all channels simultaneously, and saturates
Resolution, 0.1–10.0 keV (eV)	5–10	150–200	Currently possible
		80–100	Theoretical limit. WDS inferior to XEDS above 25 keV (suitable crystals not available)
Detector limits (weight ppm)	50–1,000	2,000–5,000	WDS used at higher beam current, fewer overlapping peaks XEDS better if current restricted (e.g., to avoid beam damage)
Accuracy of analysis (%)	± 1–2	± 6	Experimentally determined
Light element analysis (min. atomic number)	4	4	Both have ability for light element detection providing windowless or polymer window used
Rough surface work	Bad	Good	XEDS insensitive to source position

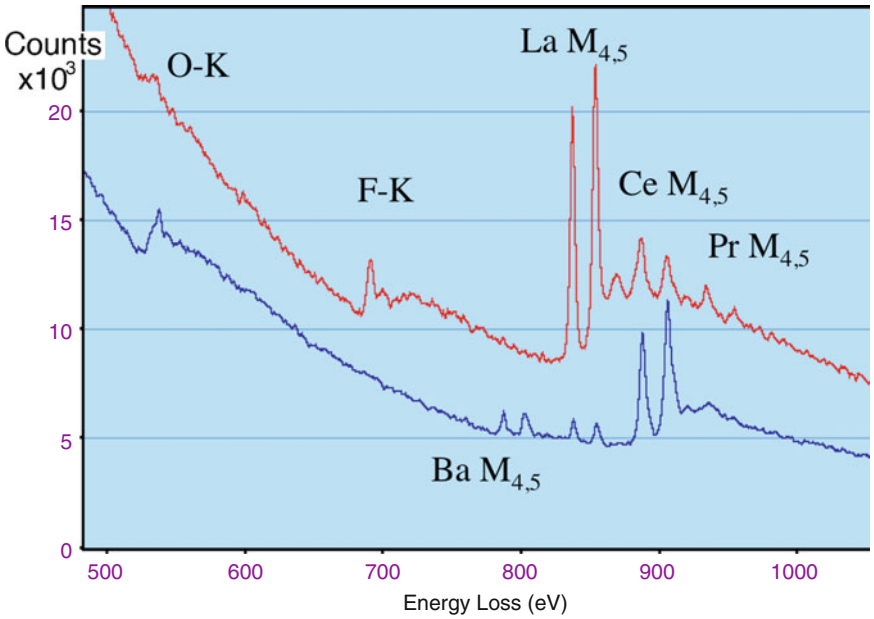

FIGURE 10.34. Example of EELS from two commercial ceria powders.

information on the bonding and chemistry of the specimen. As the beam in the TEM can now be as narrow as 0.1 nm, EELS can give highly localized information and is particularly important in ceramics where low-*Z* elements tend to be particularly important. Figure 10.34 shows part of an EELS spectrum from two commercial ceria abrasives.

The fine structure of the EELS can be compared to the fine structure in X-ray scattering. EELS can be used in purpose-built chambers or, more recently, in the TEM. In the TEM you have the great advantage of knowing where you're getting the spectrum from—it's site-specific. The difficulty with TEM, as usual, is that there are usually two surfaces to consider [you can try reflection (R) EELS—see reflection electron microscopy (REM)]. This technique will be used more in the future with the wider availability of TEM guns with smaller spread in energy. A major application for EELS, which we have only recently begun to use, is direct measurement of bonding.

10.18 ELECTRON SPECTROSCOPY

In the group of techniques known as photoelectron spectroscopy (PES), electrons are emitted from their filled electronic states in the solid by the absorption of single photons. Traditionally, the energy of the photons corresponds to the UV or X-ray wavelengths, and the techniques are known as UPS or XPS. XPS used to be called electron spectroscopy for chemical analysis, or ESCA, and is still the most-used surface-sensitive technique. The difficulty for ceramics is the usual one: as we remove electrons from the sample, the sample becomes charged and attracts the same electrons, which can distort the results. In principle, you could use a flood gun to resupply the electrons, but the challenge is getting the balance right. The techniques do explore the surface region, not just the surface, so the surface effect must be separated from the larger bulk effect. Variations of the

technique include angle-resolved photoemission spectroscopy (ARPES). These techniques are mainly used for quantitative chemical analysis of surfaces by detecting electrons emitted from the surface. They can be differentiated by how the electrons are produced. In Auger electron spectroscopy (AES), the incident species are electrons. In X-ray photoelectron spectroscopy (XPS) and UV photoelectron spectroscopy (UPS), the incident species are photons. In XPS, we illuminate the sample with X-rays and measure the energy of electrons that are then emitted. If the electrons come from regions close to the surface, we can obtain data on the chemistry and bonding close to the surface. The X-rays can be generated in a synchrotron that has both high spatial resolution and high intensity.

Auger electrons are created when an incident electron beam ionizes an atom by removing an inner-shell electron. An electron from a higher energy level fills the hole, and the resulting kinetic energy is transferred to a loosely bound electron, which is detected. These Auger electrons have relatively low kinetic energy and, consequently, a short mean free path. They come from the top 0.5–3 nm of the surface. Their energy is characteristic of the atomic energy levels of the atom from which they came. Therefore, they are sensitive surface probes of chemical composition. Auger electron spectroscopy has been used extensively to study oxide surfaces. The problem is that the surface must be very clean and examined in ultra-high vacuum.

Figure 10.35 shows examples of carbon KVV Auger electron spectra generated from the surface of two carbides, diamond, and graphite. The spectra are in the form of derivative electron yield versus electron energy and show the chemical shift effect and how this could be used for "fingerprinting" an unknown sample. AES is the spectroscopist's variation of low-energy electron diffraction (LEED) spectroscopy. Its main use is to provide information on the chemistry, rather than bonding, and more specifically to tell if the sample is clean enough for LEED. The beam can be scanned across the sample to produce an image—hence scanning Auger microscopy.

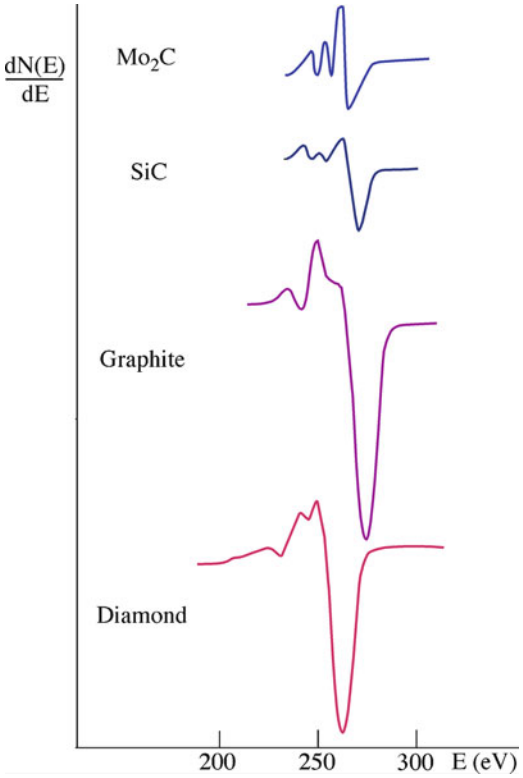

FIGURE 10.35. Derivative C KVV Auger electron spectra from two carbides, graphite, and diamond.

AUGER NOTATION

KVV refers to the series of electron transitions responsible for the Auger electron. V refers to electrons coming from the valence band of a solid.

In XPS, electrons with binding energy (E_b) are ejected from core levels by an incident X-ray photon with energy E_0. The ejected photoelectron has energy (E_0–E_b). Output electron energies are typically >10 eV. XPS, like AES, has excellent depth resolution and is sensitive to the near surface region of a material. The spectrum has the form of intensity versus binding energy.

By sputtering the surface between acquisition of either an AES or XPS spectrum, it is possible to obtain depth profiles. Sputtering must be conducted in the same system as the spectrometer to avoid contamination of the surface. UPS uses UV light to produce electrons. Using these lower photon energies (typically ~21 eV), only the valence levels are accessible. A major application of UPS is determining the band structure of solid surfaces.

10.19 NEUTRON ACTIVATION ANALYSIS

The basis of neutron activation analysis (NAA) is that if a material containing certain rare earth elements is exposed to a beam of neutrons it can become highly radioactive. If the induced radioactivity is then measured, it is possible to identify the elements that are present in the samples and quantify the amount present. The neutron interacts with the target nucleus and forms an excited nucleus; that is, the neutron loses energy. The excited nucleus then quickly relaxes back to a more stable state by emitting a characteristic γ-ray (this is an n, γ nuclear reaction). The new nucleus may be radioactive, in which case it then begins to decay by emitting additional characteristic γ-rays, but the rate of emission is slower due to the longer half-life of the decaying nucleus. Figure 10.36 gives a schema of the NAA process.

The quick emission of the γ-ray gives the technique PGNAA (prompt γ-ray NAA) and the slower emission gives the more usual technique DGNAA (delayed GNAA—but often just called NAA). Of the three principal types of neutron sources (reactors, accelerators, radioisotope neutron

emitters), nuclear reactors generating neutrons by U fission give particularly high fluxes of neutrons. Thermal neutrons have energies <0.5 eV. If the neutrons are in thermal equilibrium with the moderator of the reactor, they have a mean energy of 25 meV, which means they have a velocity of 2.2 km/s. A 1-MW reactor has a peak flux of thermal neutrons of ~10^{13} cm^{-2}/s. Table 10.12 shows how sensitive NAA is for detecting elements in a sample.

An example of an analysis: crush a sample to a fine powder; put 150 mg in a plastic vial and 200 mg in a high-purity quartz capsule. Reference samples of known composition are also prepared. The plastic vial is exposed to 5s of irradiation with a flux of 8 $\times$ 10^{13} neutrons $cm^{-2}.s^{-1}$. The γ-rays are then counted for 720 s, which gives a γ-spectrum (PGNAA) for short-lived elements: Al, Ba, Ca, Dy, K, Mn, Na, Ti, V. The samples in quartz are irradiated for 24 h with a flux of 5 $\times$ 10^{13} neutrons $cm^{-2}{\cdot}s^{-1}$. After leaving the sample for 7 days, the γ-rays are counted for 2,000 s. This middle count gives medium half-life elements: As, La, Lu, Ne, Sm, U, Y. After a further 4 weeks, the final count (9,000s) gives a measure of the long half-life elements: Ce, Co, Cr, Cs, Eu, Fe, Hf, Ni, Rb, Ru, Sb, Sc, Sr, Ta, Tb, Th, Zn, Zr. The results are then compared to those from the known material. The accuracy can be better than parts per billion.

Applications have included identifying the origin of archeological ceramics: obsidian can be fingerprinted, the trade patterns of the Olmec civilization can be followed by identifying where the clay originated that they used in their pots, and the source of contamination in semiconductors can be traced at the 1 ppb level.

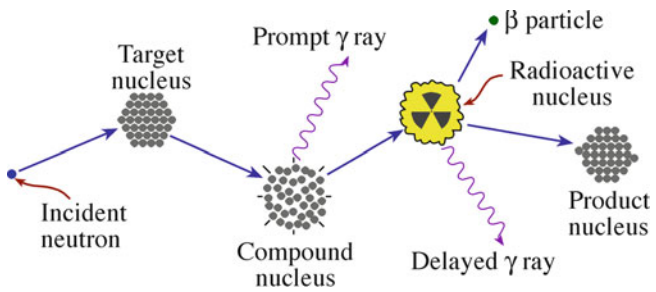

FIGURE 10.36. Neutron activation analysis (NAA) process.

TABLE 10.12 Sensitivity for Detecting Elements by NAA

Sensitivity (ng)	*Elements*
0.1	Dy, Eu
0.1–1.0	In, Lu, Mn
1–10	Au, Ho, Ir, Re, Sm, W
10–100	Ag, Ar, As, Br, Cl, Co, Cs, Cu, Er, Ga, Hf, I, La, Sb, Sc, Se, Ta, Tb, Th, Tm, U, V, Yb
100–1,000	Al, Ba, Cd, Ce, Cr, Hg, Kr, Gd, Ge, Mo, Na, Nd, Ni, Os, Pd, Rb, Rh, Ru, Sr, Te, Zn, Zr
1,000–10,000	Bi, Ca, K, Mg, P, Pt, Si, Sn, Ti, Tl, Xe, Y
10,000–100,000	F, Fe, Nb, Ne
1,000,000	Pb, S

10.20 THERMAL ANALYSIS

The term "thermal analysis" actually covers many different techniques that measure a change in a material as a function of temperature. Thermal analysis is particularly useful to characterize decomposition and crystallization during ceramic powder processing. It is then possible to determine optimum calcination temperatures. A list of the main thermal analysis techniques is given in Table 10.13. The two most common are:

- Thermogravimetric analysis (TGA)—measures weight loss during heating
- Differential thermal analysis (DTA)—measures relative changes in the sample's temperature during heating

These analyses—DTA and TGA—can be performed separately or simultaneously. Figure 10.37 shows examples of DTA and TGA analysis on an initially amorphous CA_2

TABLE 10.13 Common Thermoanalytical Techniques

Method	*Common abbreviation*	*Property measured*
Thermogravimetry	TG (TGA)	Mass
Differential thermal analysis	DTA	ΔT between sample and reference
Differential scanning calorimetry	DSC	Heat absorbed or evolved by sample
Evolved gas analysis	EGA	Nature and amount of evolved gas species
Thermodilatometry	TD	Dimension
Thermomechanical analysis	TMA	Deformation/nonoscillatory load
Dynamic thermomechanometry	DMA	Deformation/ oscillatory load
Thermomagnetometry	TM	Relative magnetic susceptibility

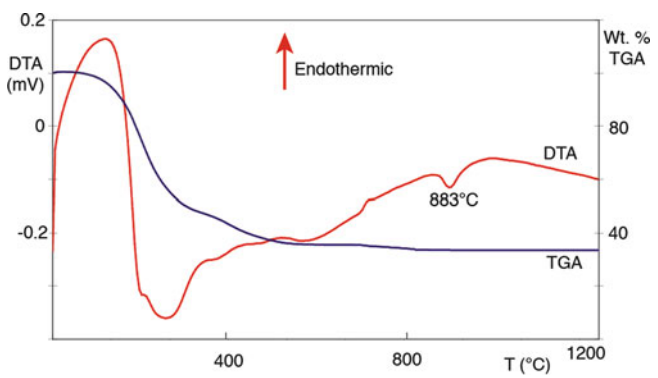

FIGURE 10.37. Differential thermal analysis (DTA) and thermogravimetric analysis (TGA) measurements show the reaction as CA_2 crystallizes.

powder as it crystallizes. The TGA plot shows that as temperature is increased the sample loses weight, and by about 600°C the weight loss is complete. The DTA plot shows that the CA_2 crystallization is exothermic.

Thermal analysis techniques are widely used to study ceramic processing. In addition to determining decomposition and crystallization process, it is possible to monitor the burnout of organic binders that are commonly added to powders prior to shaping and shrinkage during drying. One of the earliest uses for DTA was in studying clay minerals. In montmorillonite, the position of certain cations can have an influence on dehydration behavior. Analysis of DTA curves from samples of montmorillonite containing Li, Na, or K show that the presence of Li stabilizes the water of hydration, and higher temperatures are required for dehydration.

CHAPTER SUMMARY

There are many different techniques for studying ceramics. The choice of which one to use depends on the type of information that we want to obtain and how valuable our material is. TEM is destructive, but so are many other methods if we have to produce a fine powder. Although some of the techniques we described, such as VLM and SEM, are universal, there are many techniques that are available in only a few sites. Those requiring nuclear reactors of very high flux photon beams are usually found at National User Facilities.

A full understanding of a material or a process may require using several complementary techniques. For example, electron diffraction in the TEM combined with FTIR and Raman spectroscopy can unequivocally determine what polymorph of SiO_2 is present in a sample. AES can tell us the composition of the surface of a sample, AFM can give us the surface morphology, and RHEED can give us the surface crystallography.

The technological importance of nanomaterials means that we need high-resolution techniques. It is the need to understand the structure of nanomaterials and processes that occur on the atomic and molecular level that leads to the development of new instrumentation for characterizing materials.

PEOPLE AND HISTORY

Binnig, Gerd (1947–) and *Heinrich Rohrer* (1933–) of the IBM Research Laboratory in Switzerland won the Nobel Prize in Physics in 1986 for their invention of scanning tunneling microscopy (STM).

Mössbauer, Rudolf (1929–) received the Nobel Prize in Physics in 1961 for discovery of the effect.

Raman, Sir Chandrasekhara Venkata (1888–1970), the Indian scientist, discovered the phenomenon in 1928 while studying CCl_4; he was awarded the Nobel Prize in Physics in 1930.

Ruska, Ernst August Friederich was born in Heidelberg in 1906. He did his PhD with Max Knoll (who died in 1969) in Berlin, which led to the first electron microscope in 1931. He died in 1988 having shared the Nobel Prize in 1986, 55 years after the invention!

Rutherford, Ernest (1871–1937), demonstrated ion scattering, which demonstrated the utility of ions for chemical analysis. He won the 1908 Nobel Prize in Chemistry.

Stokes, George Gabriel (1819–1903) was Professor of Mathematics in Cambridge when Rayleigh was an undergraduate.

Strutt, John William (Lord Rayleigh); don't confuse the spelling with Raleigh (Sir Walter) (1842–1919). He won the Nobel Prize in Physics in 1904 for discovering Ar; succeeded James Clark Maxwell as the Cavendish Professor in Cambridge.

Synge, Edward Hutchinson (1890–1957), from Dublin, Ireland, proposed NSOM (Philos. Mag. papers 1928–1932) 50 years before it was discovered. (John Lighton Synge, a mathematician and theoretical physicist, was his younger brother).

EXERCISES

10.1 Construct a chart summarizing the principal scattering techniques used to characterize the structure, chemistry, and bonding in ceramics, emphasizing which of the three features is most directly addressed by each technique.

10.2 In Figure 10.1 the grains boundaries are described as low-angle grain boundaries. Could this information be obtained directly from VLM? If not, what other methods might have been used to make this determination?

10.3 In Figure 10.6, why does the image have a 3D appearance?

10.4 In Figure 10.7, the image distinguishes the regions with different chemistry directly and with high spatial resolution. Explain the physical process underlying this observation.

10.5 During the processing of ceramics containing crystalline quartz, a phase transformation occurs on cooling/heating between the α form and the β form. The phase transformation produces an appreciable change in volume that can lead to cracking. How would you determine from a fragment of a ceramic plate whether you had the α or β phase present in the sample?

10.6 How would you determine whether water vapor has chemisorbed onto the surface of particles of silica gel?

10.7 If we are examining steps of atomic dimensions in Figure 10.14, redraw the schematic to scale and explain the factors that determine vertical and lateral resolution in AFM.

10.8 Compare the value of NMR and Mössbauer analysis for ceramic materials.

10.9 Referring to Figure 10.33, explain why we see multiple peaks for Y and Zn occur at different energies, and why we see Cu.

10.10 Examine the DTA/TGA plots in Figure 10.37. What can you say about the curves as the temperature is increased from 25°C to 1,200°C?

10.11 Summarize the pros and cons for imaging dislocations in sapphire using X-rays and electrons. (Make at least five points for and against each being quantitative, when possible).

10.12 What is the best resolution possible today using SEM? Why do we sometimes use lower voltages even if it means lower resolution?

10.13 Why or when does SEM give a greater depth of field than VLM?

11.14 Which imaging mode (using BSEs or SEs) would you use to image: (1) steps on sapphire, (2) Pt particles on ceria, (3) the structure of a glass/crystal mixture, and (4) the texture of polycrystalline zirconia?

10.15 If the different gray levels in Figure 10.10A correspond to different thicknesses, what can you deduce about the geometry of this sample?

10.16 Show how the contrast in Figure 10.11 matches the structure of the crystal; label two independent directions and two edge-on planes.

10.17 Do the spacings of the fringes in Figure 10.12 match those expected for these materials?

10.18 The caption in Figure 10.16 says the steps are 0.4 nm high. Explain and justify this statement and assess its accuracy.

10.19 Mössbauer spectroscopy of rare earth elements such as Nd, Eu, and Dy attracts considerable attention from physicists. Should ceramists be equally interested in these elements and why is Mössbauer spectroscopy a good technique to study them? Briefly explain your answer.

10.20 NMR is a favorite technique of chemists but not as popular with ceramists. Discuss the veracity of this state. Should it and will it change?

GENERAL READING

Cahn RW (2005) Concise encyclopedia of materials characterization, 2nd edn. Elsevier, Amsterdam, A good place to check out any technique

Chu WK, Mayer JW, Nicolet MA (1980) Backscattering spectrometry. Academic, New York, Detailed information about RBS

Hartshorne NH, Stuart A (1970) Crystals and the polarizing microscope, 4th edn. Arnold, London

Hollas JM (2004) Modern spectroscopy, 4th edn. Wiley, Chichester, Covers a wide range of topics at the level you'll need if you use the techniques

Loehman RE (ed) Characterization of ceramics, (republished in 2010 by Momentum Press). Provides "case studies" where various techniques are used.

Wachtman JB (1992) Characterization of materials. Butterworth-Heinemann, Boston, Overview and comparison of the different characterization techniques

SPECIFIC REFERENCES

Binnig G, Rohrer H, Gerber Ch, Weibel E (1982) Tunneling through a controllable vacuum gap. Appl Phys Lett 40:178, Paper describing the STM

Blanpain B, Revesz P, Doolittle LR, Purser KH, Mayer JW (1988) The use of the 3.05 MeV oxygen resonance for He-4 backscattering near-surface analysis of oxygen-containing high Z compounds. Nucl Instrum Methods B34:459, Describes the RBS method used to obtain the enhanced oxygen signal

Philp E, Sloan J, Kirkland AI, Meyer RR, Friedrichs S, Hutchison JL, Green MLH (2003) An encapsulated helical one-dimensional cobalt iodide nanostructure. Nature Materials 2:788

Raman CV, Krishnan KS (1928) A new type of secondary radiation. Nature 121:501, The original description of the "Raman Effect"

Standard test method for interstitial atomic oxygen content of silicon by infrared absorption. F 121. Annual Book of ASTM Standards, Vol 10.05, ASTM, Philadelphia, pp 240–242.